

Research Article

Andrographolide Suppresses Pyroptosis in *Mycobacterium tuberculosis*-Infected Macrophages via the microRNA-155/Nrf2 Axis

Yan Fu ¹, Jingjing Shen,¹ Fanglin Liu,¹ Hemin Zhang,¹ Yuejuan Zheng ^{1,2,3},
and Xin Jiang ¹

¹Center for Traditional Chinese Medicine and Immunology Research, School of Basic Medical Sciences, Shanghai University of Traditional Chinese Medicine, Shanghai 201203, China

²The Research Center for Traditional Chinese Medicine, Shanghai Institute for Major Infectious Diseases and Biosafety, Shanghai 200032, China

³Shanghai Key Laboratory of Health Identification and Assessment, Shanghai University of Traditional Chinese Medicine, Shanghai 201203, China

Correspondence should be addressed to Yuejuan Zheng; 13641776412@163.com and Xin Jiang; jiangxingao@163.com

Received 14 December 2021; Accepted 11 April 2022; Published 28 April 2022

Academic Editor: Daniel Dias Rufino Arcanjo

Copyright © 2022 Yan Fu et al. This is an open access article distributed under the Creative Commons Attribution License, which permits unrestricted use, distribution, and reproduction in any medium, provided the original work is properly cited.

Tuberculosis (TB) remains a leading threat to public health worldwide with *Mycobacterium tuberculosis* (Mtb) infections causing long-term abnormal and excessive inflammatory responses, which in turn lead to lung damage and fibrosis, and ultimately death. Host-directed therapy (HDT) has been shown to be an effective anti-TB strategy in the absence of effective anti-TB drugs. Here, we used an *in vitro* macrophage model of Mtb infection to evaluate the effects of andrographolide (Andro), extracted from *Andrographis paniculata*, on pyroptosis in Mtb-infected macrophages. We evaluated the molecular mechanisms underlying these outcomes. These evaluations revealed that Andro downregulated the expression of proinflammatory miR-155-5p, which then promoted the expression of Nrf2 to suppress pyroptosis in Mtb-infected macrophages. Further study also demonstrated that siNrf2 could attenuate the inhibitory effect of Andro on TXNIP, validating our mechanistic studies. Thus, our data suggest that Andro may be a potential candidate adjuvant drug for anti-TB therapy as it inhibits pyroptosis in Mtb-infected macrophages, potentially improving clinical outcomes.

1. Introduction

Despite extensive intervention, tuberculosis (TB) remains one of the most lethal infectious diseases in the world, and although there are several first-line drugs for the treatment of TB, they generally have several shortcomings, including long treatment cycles and major side effects. Moreover, the severe inflammatory damage resulting from active TB infection can also reduce the treatment efficiency. The last several decades have witnessed a substantial effort to develop novel anti-TB drugs, but the outcomes of these studies remain unsatisfactory. The major problems associated with this development include slow progress in devel-

oping anti-TB drugs and inevitable drug resistance of TB [1]. Therefore, a novel strategy for treating TB is urgently required.

Current researches suggest that most TB patients do not die directly from *Mycobacterium tuberculosis* (Mtb) infection, but rather from the tissue damage induced by the long-term excessive inflammatory response associated with these infections [2, 3]. Moreover, excessive inflammatory responses also promote the spread of Mtb and reduce treatment efficacy [4]. This implies that avoiding the excessive immune response of the body can reduce the risk of death in TB patients and enhance the efficacy of anti-TB drugs, making it a novel target for interventional strategies.

Host-directed therapy (HDT) is a novel adjuvant therapy against TB which is designed to use drugs to regulate the protective immune response against the pathogen and reduce excessive inflammation in the infected tissues [5]. HDT drugs can help the host to reduce the excessive inflammatory response in Mtb-infected macrophages, which act as the primary effector cells for the elimination of Mtb [6], thus alleviating tissue damage and improving the treatment efficiency of the anti-TB drugs [7].

Pyroptosis is a proinflammatory form of programmed cell death and has been shown to induce excessive inflammatory responses in affected tissues resulting in serious tissue damage and pathological progression [8]. In TB, pyroptosis in Mtb-infected macrophages not only releases several pro-inflammatory mediators, including high mobility group protein (HMGB1) and interleukin-1 β (IL-1 β), but also spreads the Mtb bacteria, aggravating the pathologic process and increasing the risk of infection [9–11].

microRNAs (miRNAs) are noncoding transcripts of 18–25 nucleotides, which interact with the 3'-untranslated regions (3'-UTRs) of their targets mRNAs resulting in their degradation or inhibition of their translation [12, 13]. Since the initial discovery of their regulatory role in the development of the nematodes, miRNAs have emerged as key modulators in many biological processes, including the inflammatory response [14, 15]. Studies have revealed that there are a variety of key miRNAs associated with infection and disease progression. One example is miR-155-5p which acts as a proinflammatory miRNA participating in several infectious diseases [16, 17]. Furthermore, research also has shown that miR-155-5p is upregulated in macrophages infected with Mtb [18, 19]. It has also been demonstrated that multiple miRNAs can modulate the same target, and a single miRNA can modulate multiple targets [20, 21]. In addition, studies have demonstrated that miR-155-5p regulates several genes, including suppressor of cytokines signaling1 (SOCS1), silent information regulator 1 (Sirt1), autophagy-related gene 12 (ATG12), and nuclear factor erythroid 2-related factor 2 (Nrf2) [22–25], which might ameliorate the inflammatory response [26–29].

Nrf2 is an essential regulator of the antioxidant response [30, 31]. Oxidative stress stabilizes Nrf2 protein expression and initiates the activation of a multistep pathway that includes its nuclear translocation, recruitment of transcriptional coactivators, and subsequent binding of antioxidant response elements within its target genes [32, 33]. Several studies have revealed that activation of the Nrf2/HO-1 signaling pathway could contribute to the inhibition of oxidative stress induced pyroptosis [34], while other studies have shown that it can also attenuate pyroptosis by suppressing the activation of the NLRP3 inflammasome [35, 36].

Andrographolide (Andro) is the major bioactive component of *Andrographis paniculata*, which is known to exert several biological effects, including anti-inflammatory, anti-tumor, antiviral, and antioxidant effects [37–40]. Moreover, treatment with Andro can activate Nrf2 promoting HO-1 expression and suppressing oxidative stress and neuroinflammation in primary astrocytes [41]. Our previous study has also revealed that Andro treatment can inhibit the

inflammatory response in Mtb-infected macrophages [42]. Given that traditional Chinese medicines generally have applications against multiple targets, we speculate that Andro could also inhibit the inflammatory response using other pathways. Moreover, recent publications have revealed that Andro treatment suppresses pyroptosis via inhibiting the activation of the AIM2 inflammasome [37]. However, to our knowledge, there is no relevant report discussing whether Andro treatment might suppress macrophage pyroptosis via the miR-155/Nrf2 axis. Here, we describe a novel mechanism of Andro and demonstrate that it could be used as an adjuvant drug against TB to alleviate excessive inflammatory response via suppression of Mtb-infected macrophage pyroptosis.

2. Materials and Methods

2.1. Chemicals and Reagents. Western and IP lysis buffer, BCA protein assay kit, protein A/G agarose/sepharose beads, and propidium iodide (PI) were bought from the Beyotime Institute of Biotechnology (Shanghai, China). The following antibodies were used: anti-Nrf2 (12721), anti-HO-1 (43966), and anti-NLRP3 (15101S) were bought from Cell Signaling Technology, Inc.; anti-GSDMD (A20197), anti-Histone3 (A2348), and goat anti-NLRP3 (A14223) were obtained from ABclonal Technology (Wuhan, China); and anti-TXNIP (sc-166234) and anti-TRX2 (sc-133201) were obtained from Santa Cruz Biotechnology, Inc. Middlebrook 7H9 and 7H10 media were purchased from Difco (Detroit, MI, USA); oleic acid-albumin-dextrose-catalase (OADC) supplements were obtained from BD Biosciences (BD, Sparks, MD, USA). RiboFECT CP transfection kit, mouse miR-155-5p mimic (miR1CM001), mouse mimic NC #22 (miR1N0000001-1-5), mouse miR-155-5p inhibitor (miR20000165-1-5), mouse inhibitor NC #24 (miR2N0000002-1-5), mouse miR-155-5p antagomir (miR31148164306-4-5), and mouse antagomir NC #24 (miR3N0000002-4-5) were obtained from Ribo Biotechnology (Guangzhou, China). IL-1 β ELISA kit was bought from R&D (USA). NE-PER™ nuclear and cytoplasmic extraction reagent kit (78833) and SuperSignal™ West Femto maximum sensitivity substrate (34096) were bought from Thermo Fisher Scientific (USA). EZ-press RNA purification kit was obtained from EZBioscience. PrimeScript™ RT reagent kit (RR037A and RR036A) and SYBR RT-PCR kits were purchased from Takara Shuzo, Otsu (Japan). RT-PCR primers were purchased from Sangon Biotech (Shanghai, China).

2.2. Animals. Male C57BL/6J mice (6–8 weeks, 20 \pm 3 g) were obtained from Vital River Laboratory Animal Technology Co., Ltd. (Beijing, China). Animal experiments strictly follow the National Institute of Health Guide for the Care and Use of Laboratory Animals, with the approval of the Scientific Investigation Board of Shanghai University of Traditional Chinese Medicine (Shanghai, China).

2.3. Drugs. Andrographolide (Andro) (molecular weight: 350.45, purity >98%) is isolated from *Andrographis paniculata* (the full names of drug have been checked according to <http://www.theplantlist.org/>). Andro was obtained from

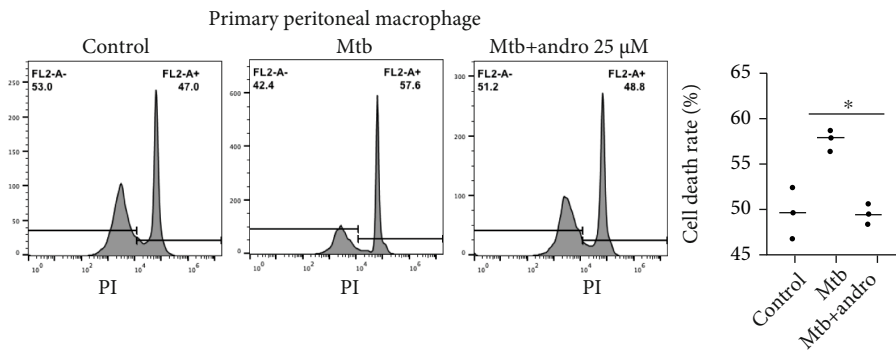
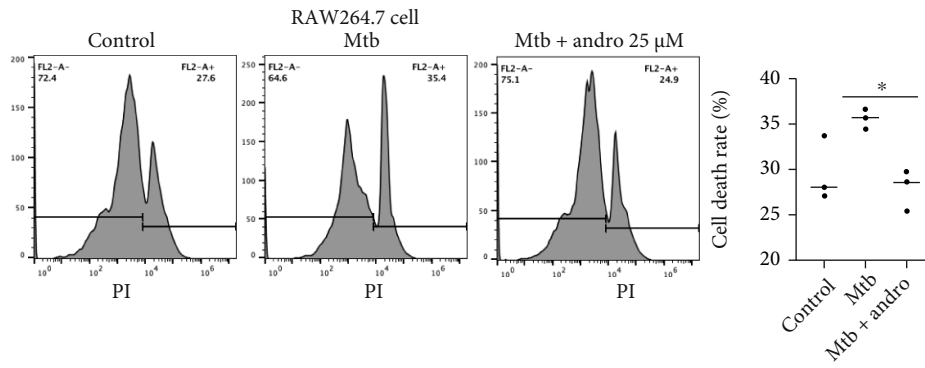
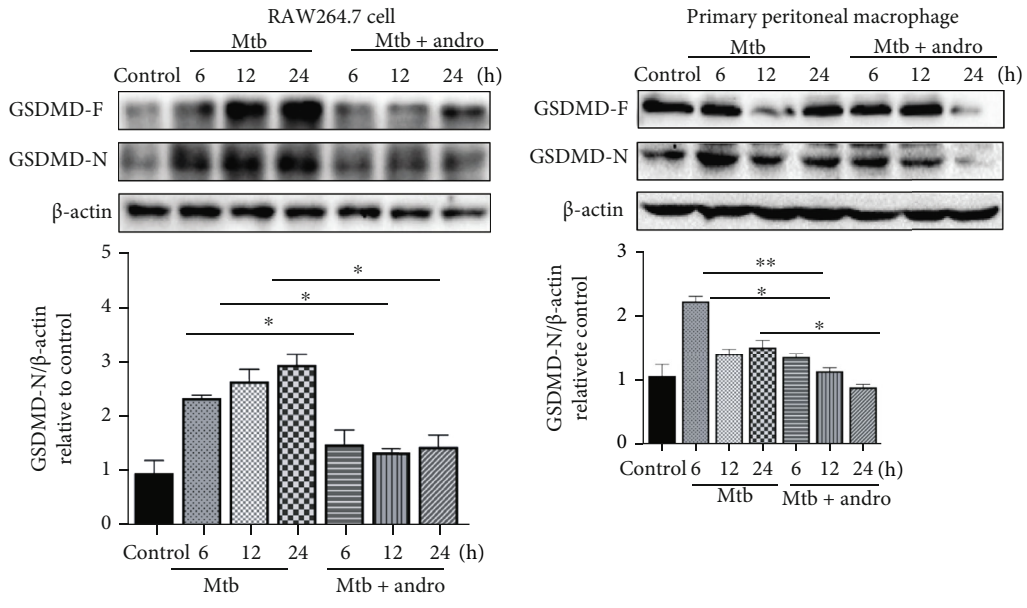


FIGURE 1: Continued.

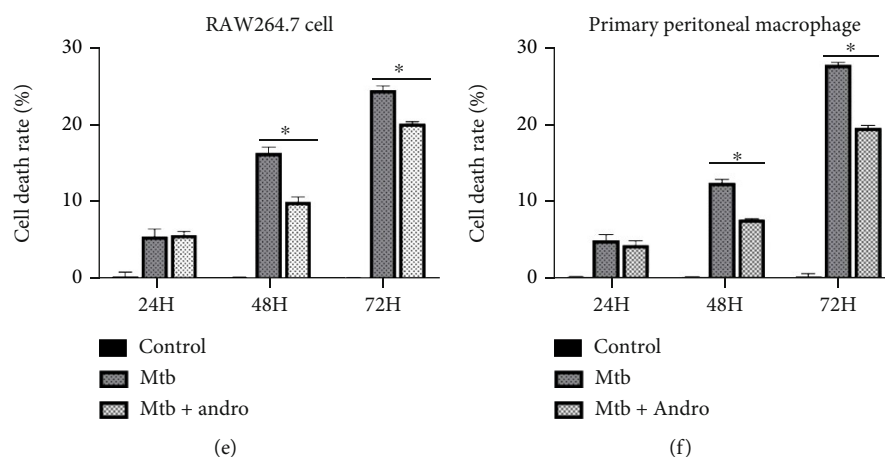


FIGURE 1: Andro ameliorates pyroptosis in Mtb-infected macrophages. (a, b) Levels of GSDMD-N protein were detected by western blotting in RAW264.7 cells and primary peritoneal macrophage cells, respectively. (c, d) The viable and dead cell populations were measured by PI staining in RAW264.7 cells and primary peritoneal macrophage cells, respectively. FL2-A+ represents the dead cell populations; FL2-A- represents the viable cell populations. (e, f) Cell death was detected by using the lactate dehydrogenase (LDH) cytotoxicity assay kit in RAW264.7 cells and in primary peritoneal macrophage cells, respectively. Data are shown as mean \pm SD of three independent experiments. * $p < 0.05$, ** $p < 0.01$.

Shanghai Tauto Biotech Co., Ltd. (CAS:5508-58-7) (Shanghai, China).

2.4. Cell Culture. Mouse macrophage-like cell line Raw264.7 was obtained from ATCC (Manassas, VA) and cultured in DMEM supplemented with 10% fetal bovine serum (FBS) in 5% CO₂ at 37°C as described previously [43]. Thioglycolate-elicited mouse primary peritoneal macrophages were prepared from male C57BL/6J mice (6-8 weeks of age) as described previously [44].

2.5. Bacterial Strains. The Mtb H37Ra was used in this study. H37Ra strain was grown in Middlebrook 7H9 or 7H10 broth supplemented with 0.2% glycerol, 0.05% Tween-80, and 10% Middlebrook OADC supplement.

2.6. Mtb Infection. The cells were seeded at the appropriate cell culture plates and grown at 37°C overnight. The cells were infected with Mtb H37Ra at a MOI (multiplicity of infection) of 10:1. After 4 h of co-incubation at 37°C, cells were washed three times with sterile phosphate-buffered saline (PBS) and cultured with DMEM containing 10% FBS in the presence and absence of Andro (25 μ M) for different times as described previously [43].

2.7. Western Blotting. The cells were lysed in lysis buffer after incubation with or without Andro (25 μ M) for different times (6, 12, and 24 hours). Then, BCA protein assay kit was used to determine the total protein concentration of each sample. Then, 5 \times SDS loading buffer was added to the whole cell lysate followed by boiled 10 min, and then, the proteins were separated by SDS-PAGE and transferred onto nitrocellulose membranes followed by blocking with 5% (w/v) bovine serum albumin and incubated with specific primary antibodies at 4°C overnight. Then, the membranes were washed with TBST for three times followed by incubation with HRP-conjugated secondary antibodies at room

temperature for 1 hour. Chemiluminescence was tested with ECL-chemiluminescent kit (Thermo Scientific). The quantification of each protein was performed by Image J-1.51(100) (2015) as described previously [43].

2.8. RNA Quantification. The Raw264.7 cells or primary peritoneal macrophage cells were seeded at 6-well cell culture plates and grown at 37°C overnight. The cells were infected with Mtb H37Ra (MOI = 10:1). Then, the cells were washed three times with sterile PBS after 4 hours and cultured with DMEM containing 10% FBS in the presence and absence of Andro (25 μ M) for 6, 12, and 24 hours. The total RNA, including miRNA, was extracted with EZ-press RNA purification kit according to the manufacturer's instruction. The miRNA and mRNAs were reverse transcribed using PrimeScript™ RT reagent kit (Takara, RR037A) and PrimeScript™ RT reagent kit (Takara, RR036A), respectively. Real-time quantitative RT-PCR analysis was performed by the SYBR RT-PCR kits. The relative expression level of miR-155-5p and mRNAs was normalized to that of internal control U6 and β -actin, respectively, by using a $2^{-\Delta\Delta C_t}$ cycle threshold method. cDNA from various cell samples was amplified with specific primers (Mouse-miR-155-5p: Forward 5'-GCGCGTTAATGCTAATTGTGAT-3' and Reverse 5'-AGTGCAGGGTCCGAG GTATT-3', RT 5'-GTCGTATCCAGTGCAGGGTCCGAGGTATTCCGACTG GAT ACGACACCCCT-3'; Mouse-U6: Forward 5'-GCTTCG GCAGCACATATACTAA AAT-3' and Reverse 5'-CGCTTC ACGAATTTGCGTGTGCAT-3', RT 5'-CGCTTCAC GAAT TTGCGTGTGCAT-3'; Mouse-miR-155HG: Forward 5'-TTTG GCCTCTGACT GACTCCTACC-3' and Reverse 5'-GTTC ATCCAGCAGGGTGACTCTTG-3'; Mouse-Nrf2: Forward 5'-CAGCATAGACAGGACATGGAG-3' and Reverse 5'-GAA CAGCGGTAGTATCAGCCAG-3'; Mouse-HO-1: Forward 5'-CACTCTGGAGATG ACACCTGAG-3' and Reverse

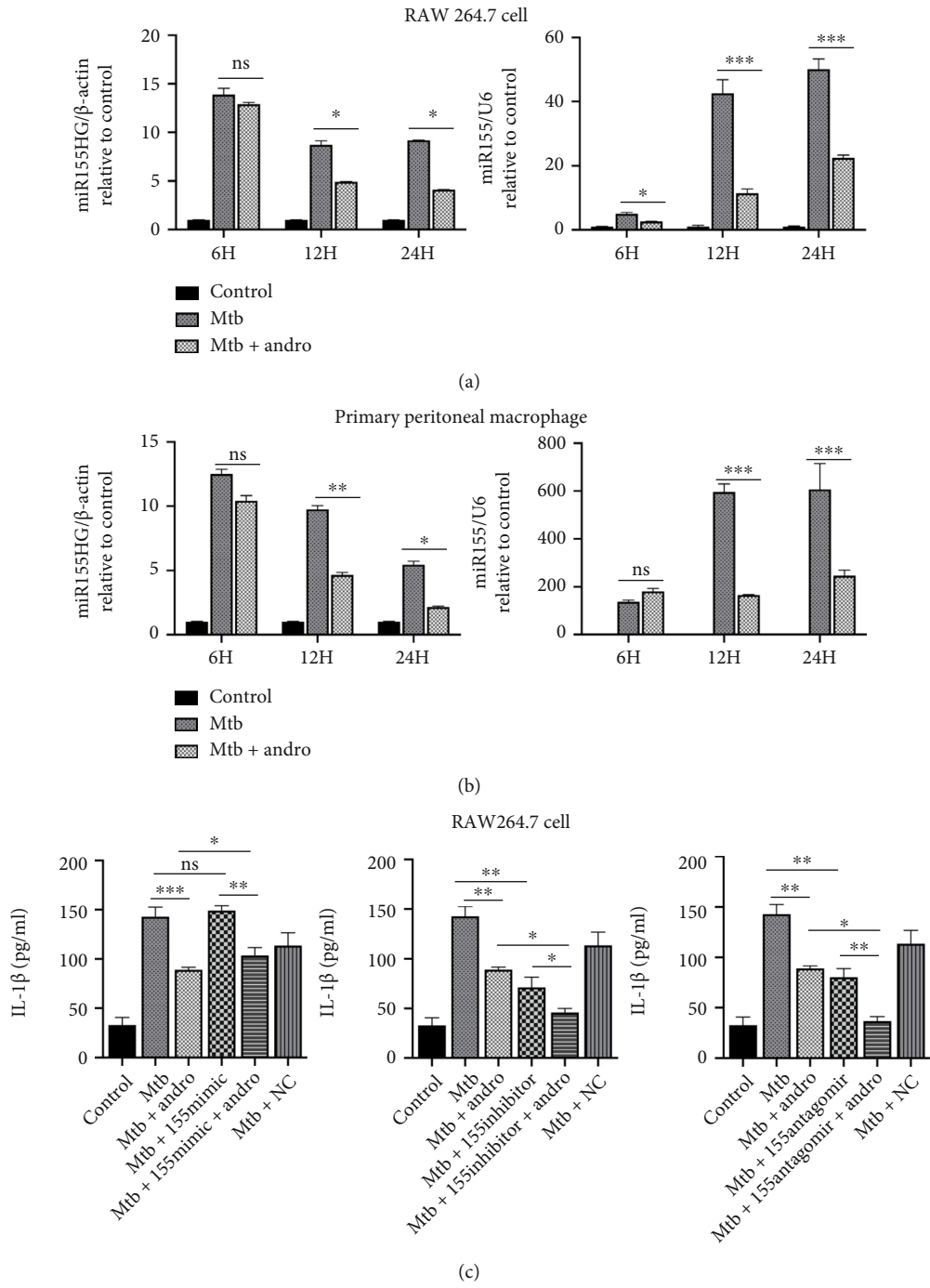


FIGURE 2: Continued.

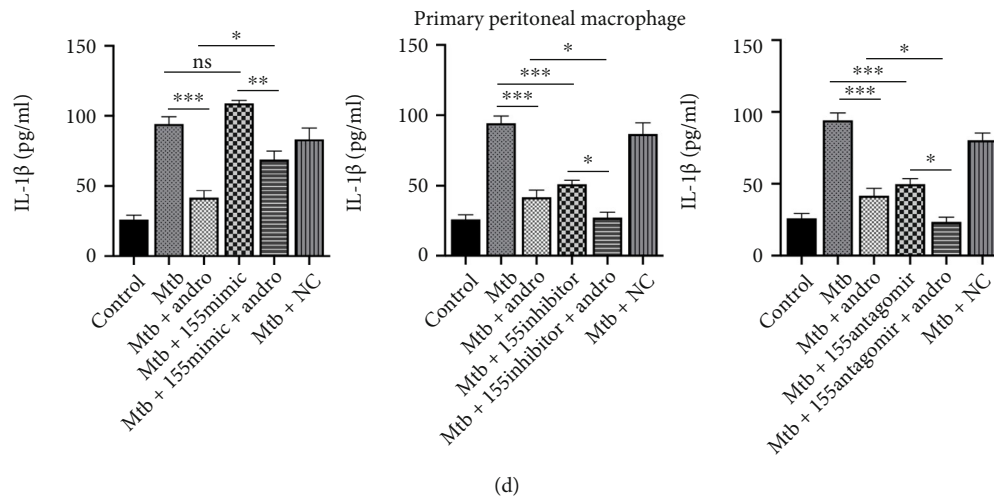


FIGURE 2: Andro inhibits pyroptosis in Mtb-infected macrophages through suppressing miR-155HG/miR-155-5p. (a, b) The expression of miR-155HG and miR-155-5p was analyzed by RT-PCR in RAW264.7 cells and primary peritoneal macrophage cells, respectively. (c, d) Levels of IL-1 β determined by ELISA measurement in macrophage cells and primary peritoneal macrophage cells, respectively. Data are shown as mean \pm SD of three independent experiments. NC: negative control. * $p < 0.05$, ** $p < 0.01$, *** $p < 0.001$. ns: nonsignificant.

5'-GTGTTCTCTGTCAGCATCACC-3'; Mouse-NQO-1: Forward 5'-GCCGAACACAAGAAGCTGGAAG-3' and Reverse 5'-GGCAAATCCTGCTACGAGCACT-3'; Mouse- β -actin: Forward 5'-CATTGCTGA CAGGATGCAGAAGG-3' and Reverse 5'-TGCTGGAAGGTGGACAGTGAGG-3').

2.9. Coimmunoprecipitation. The cells were seeded at 35 mm dishes and infected with Mtb H37Ra (MOI = 10:1) after adherence. Then, PBS was used to wash the cells for three times after 4 hours and followed by cultured with or without Andro (25 μ M) for 12 hours. The cells were lysed by lysis buffer and centrifugated (12000 rpm, 10 min). Samples containing equal amounts of protein were incubated with specific antibodies overnight at 4°C with gentle rotation. Then, the samples were added with protein A/G agarose/sepharose beads at 4°C with gentle rotation 4 hours followed by washing with lysis buffer four times. The samples were boiled in 1 \times SDS buffer before SDS-PAGE electrophoresis. The steps after SDS-PAGE electrophoresis are the same as western blotting measurement as described previously [43].

2.10. Immunofluorescence. The cells were seeded at culture plates and grown at 37°C overnight. Then, the cells were infected with Mtb H37Ra (MOI = 10:1). Then, the cells were washed three times with sterile PBS after 4 hours and cultured with DMEM containing 10% FBS in the presence and absence of Andro (25 μ M) for 12 hours. The cells were washed with PBS for three times and fixed with 4% paraformaldehyde at room temperature for 15 min. The fixed cells were washed three times with PBS and permeabilized with 2% of Triton X-100 for 15 min at room temperature. Then, the cells were blocked with 5% bovine serum albumin for 0.5 hours at room temperature followed by staining with primary antibodies 4°C overnight. Then, the cells were washed three times with PBS followed by incubation with secondary antibodies for 2 hours. Then, the cells were washed with PBS

for three times followed by staining with DAPI for 10 min. Fluorescence images were acquired on the Zeiss confocal microscopy system as described previously [43].

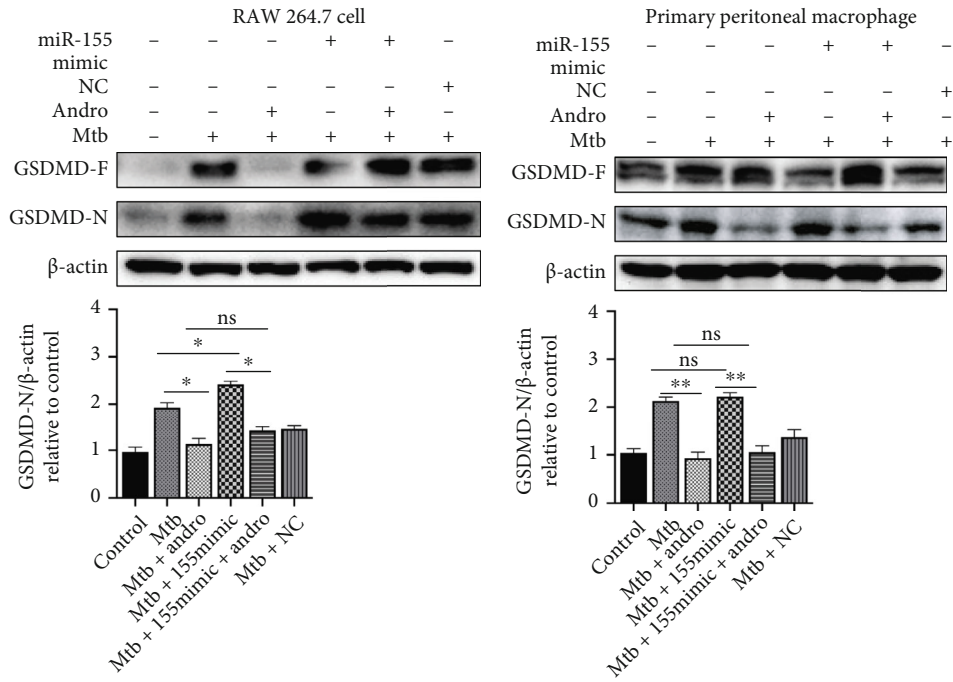
2.11. LDH Release Assay. The lactate dehydrogenase (LDH) cytotoxicity assay kit was used to assess the cell death level. The cells were seeded at 24-well plates and grown at 37°C overnight. Then, Mtb H37Ra (MOI = 10:1) was used to infect the cells. After incubation for 4 hours, the cells were washed with PBS for three times followed by addition with or without Andro (25 μ M) medium. The cell supernatant was collected and centrifuged (1000 rpm, 5 min) after incubation appropriate times. Then, the LDH levels were determined according to the manufacturer's protocol as described previously [43].

2.12. IL-1 β ELISA. The cells were seeded at 24-well plates and grown at 37°C overnight. Then Mtb H37Ra (MOI = 10:1) was used to infect the cells. After incubation 4 hours, the cells were washed with PBS with three times and followed by addition with or without Andro (25 μ M) medium. Then, the supernatants of the cells were collected and applied enzyme-linked immunosorbent assay (ELISA) kits to assess the level of IL-1 β according to the manufacturer's protocol as described previously [43].

2.13. PI Staining. The cells were infected with Mtb H37Ra (MOI = 10:1), washed with PBS for three times after 4 hours incubation, and followed by addition with or without Andro (25 μ M) medium.

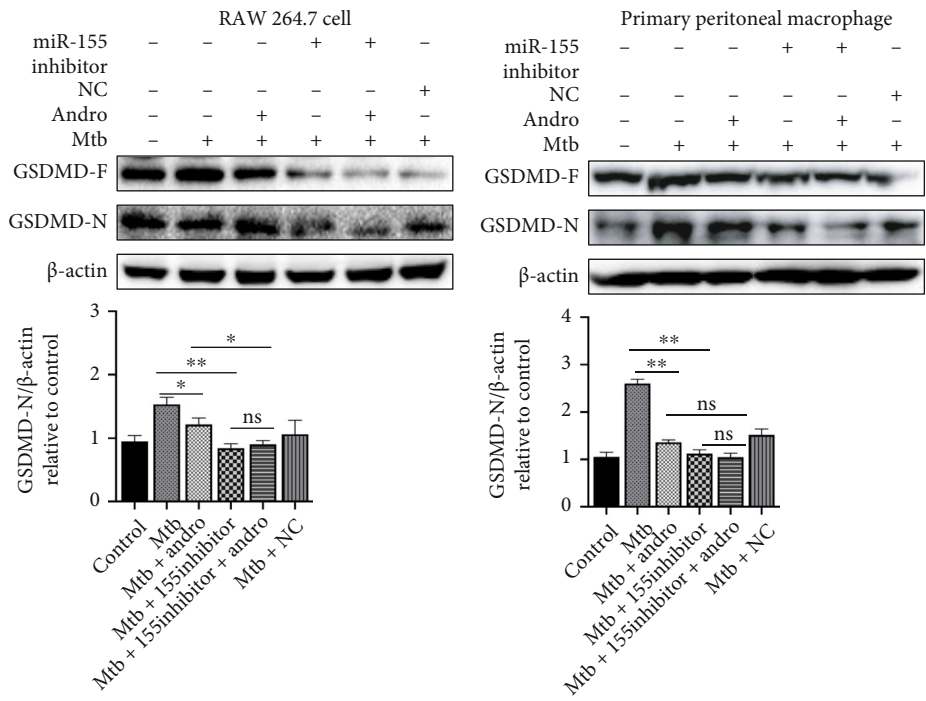
Then, the cells were collected and followed by staining with 2 μ g/ml propidium iodide (PI) for 10 min. Cell death rates were measured by C6 flow cytometer (BD Accuri™) as described previously [43].

2.14. RNA Interference. The cells were transfected with 20 μ M siRNA, 50 μ M miR-155-5p mimic, miR-155-5p inhibitor, or 100 μ M miR-155-5p antagomir for 24 hours.



(a)

(b)



(c)

(d)

FIGURE 3: Continued.

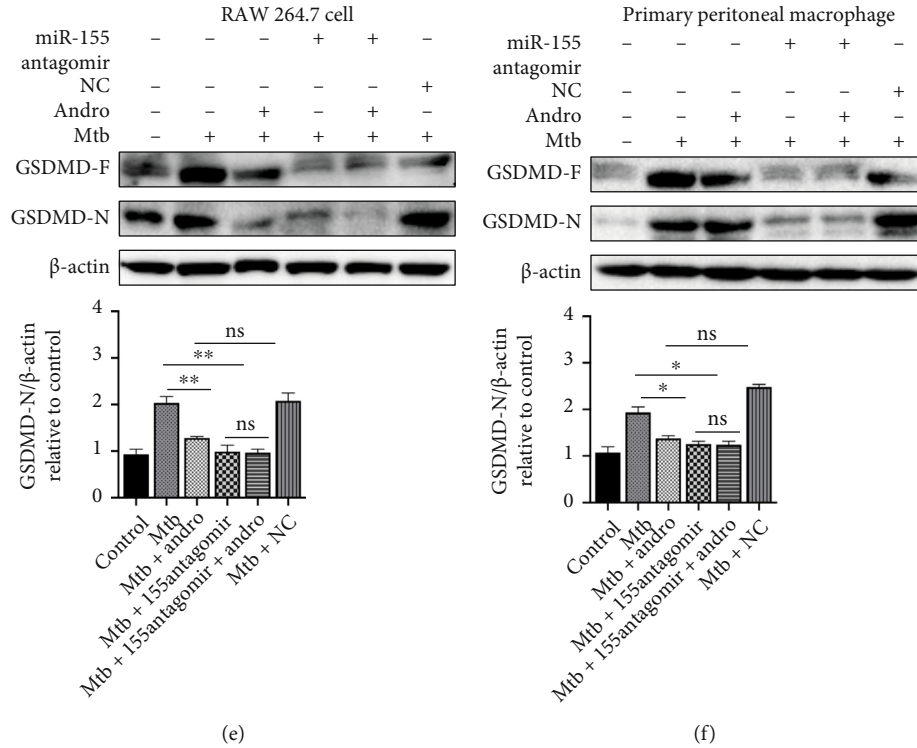


FIGURE 3: Andro inhibits pyroptosis in Mtb-infected macrophages through suppressing miR-155HG/miR-155-5p. (a, b) Levels of GSDMD-N were assessed by western blotting after miR-155-5p mimic transfection in RAW264.7 cells and primary peritoneal macrophage cells, respectively. (c, d) The expression of GSDMD-N was investigated by western blotting after miR-155-5p inhibitor transfection in RAW264.7 cells and primary peritoneal macrophage cells, respectively. (e, f) The expression of GSDMD-N was investigated by western blotting after miR-155-5p antagomir transfection in RAW264.7 cells and primary peritoneal macrophage cells, respectively. Data are shown as mean \pm SD of three independent experiments. NC: negative control. * $p < 0.05$, ** $p < 0.01$. ns: nonsignificant.

Then, the cells were infected with Mtb H37Ra (MOI = 10:1) and washed with PBS for three times followed by addition with or without Andro (25 μ M) medium after 4 hours. Then, the cells were collected after incubation for appropriate times followed by western blotting or RT-PCR analysis. The siRNA sequences are as follows:

Nrf2-mus-931 (KD1) sense 5'-GCAACUGUGGUCCA CAUUTT-3',
 Antisense 5'-AAAUGUGGACCACAGUUGCTT-3';
 Nrf2-mus-793 (KD2) sense 5'-CCGAAUUACAGUGU CUUAATT-3',
 Antisense 5'-UUAAGACACUGUAAUUCGGTT-3';
 Nrf2-mus-275 (KD3) sense 5'-GCAGGACAUGGAUU UGAUUTT-3',
 Antisense 5'-AAUCAAAUCCAUGUCCUGCTT-3';
 Negative control sense 5'-UUCUCCGAACGUGUCA CGUTT-3',
 Antisense 5'-ACGUGACACGUUCGUAGAATT-3'.
 The mus-miR-155-5p mimic was 5'-UUAAUGC UAAU UGUGAUAGGGGU-3'.

2.15. Statistical Analysis. GraphPad Prism 8 (GraphPad Software, La Jolla, CA, USA) was used to statistical analysis. Statistical significance was performed using one-way ANOVA

analysis, and results were given as the means \pm standard deviation (SD). Data shown are representative of at least triplicate experiments. $p < 0.05$ was considered to be statistically significant.

3. Results

3.1. Andro Ameliorates Pyroptosis in Mtb-Infected Macrophages. Given the role of pyroptosis in inflammation, we hypothesized that Andro may reduce inflammation in TB by suppressing pyroptosis in Mtb-infected macrophages. Here, we used Mtb to infect RAW264.7 cells and primary peritoneal macrophage cells to produce an appropriate set of experimental models. According to a previous MTT measurement [42], we used 25 μ M Andro to treat Mtb-infected macrophages and then assessed GSDMD-N levels using western blotting. The results showed that Mtb infection induced the cleavage of GSDMD, while Andro treatment significantly downregulated the expression of GSDMD-N (Figures 1(a) and 1(b)).

We also used propidium iodide (PI) staining and flow cytometric assay to determine whether Andro treatment affected the viability of macrophages and demonstrated that Mtb increased the death rate in infected macrophages, while Andro treatment significantly reduced this effect (Figures 1(c) and 1(d)).

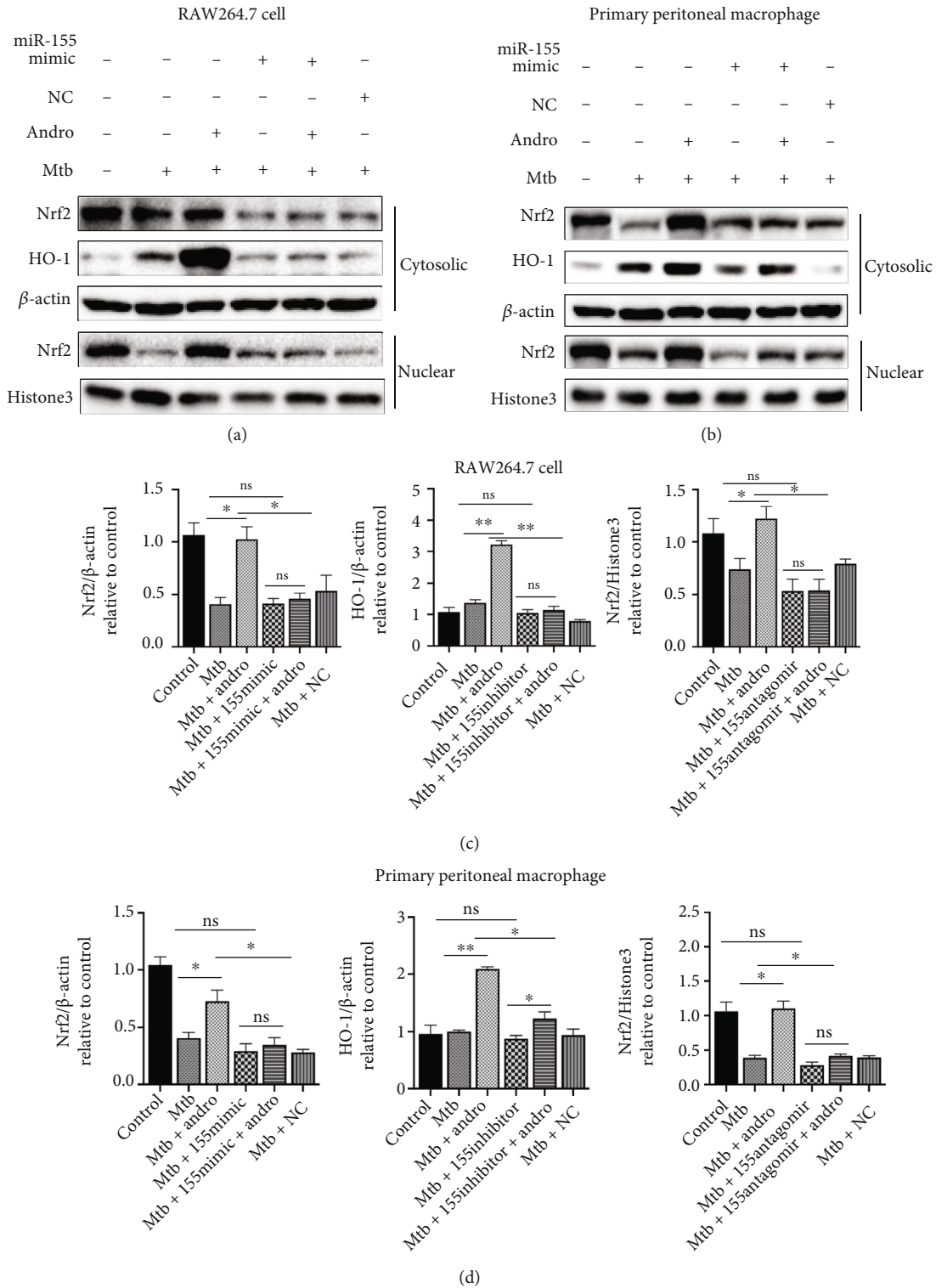


FIGURE 5: miR-155-5p mimic downregulates the expression of Nrf2 and HO-1 in Mtb-infected macrophages. (a, c) The expressions of Nrf2 and HO-1 were analyzed by western blotting after miR-155-5p mimic treatment in RAW264.7 cells. (b, d) The levels of Nrf2 and HO-1 proteins were assessed by western blotting after miR-155-5p mimic treatment in primary peritoneal macrophage cells. Data are shown as mean \pm SD of three independent experiments. NC: negative control. * $p < 0.05$, ** $p < 0.01$. ns: nonsignificant.

Lactate dehydrogenase (LDH) is a relatively stable enzyme released during cell death and is often used as an adjuvant marker of pyroptosis [45]. Based on this, we evalu-

ated LDH levels in these cells in an effort to assess the level of pyroptosis. Both macrophage models revealed that Mtb infection induced increased cell death over time, while

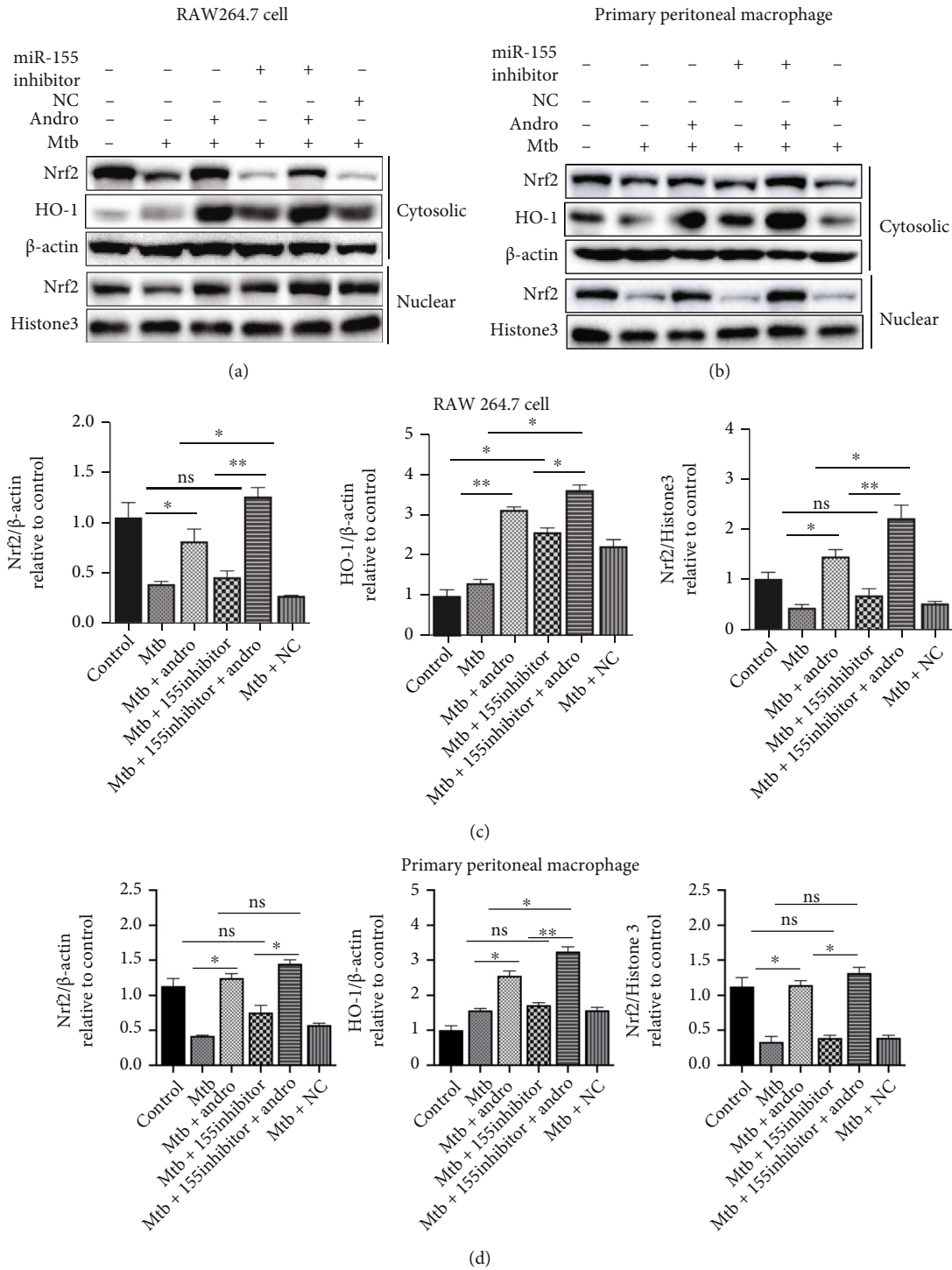


FIGURE 6: miR-155-5p inhibitor upregulates the expression of Nrf2 and HO-1 in Mtb-infected macrophages. (a, c) The expressions of Nrf2 and HO-1 were analyzed by western blotting after miR-155-5p inhibitor treatment in RAW264.7 cells. (b, d) The levels of Nrf2 and HO-1 proteins were assessed by western blotting after miR-155-5p inhibitor treatment in primary peritoneal macrophage cells. Data are shown as mean \pm SD of three independent experiments. NC: negative control. * $p < 0.05$, ** $p < 0.01$. ns: nonsignificant.

Andro treatment reduced this trend (Figures 1(e) and 1(f)). This is consistent with our previous findings, which demonstrated that Andro treatment of Mtb-infected macrophages reduces IL-1 β level, suggesting a decrease in proinflammatory cytokines. Taken together, these results indicate that

Andro treatment ameliorates pyroptosis in Mtb-infected macrophages.

3.2. Andro Inhibits Pyroptosis in Mtb-Infected Macrophages via Suppression of miR-155HG/miR-155-5p. Several researches

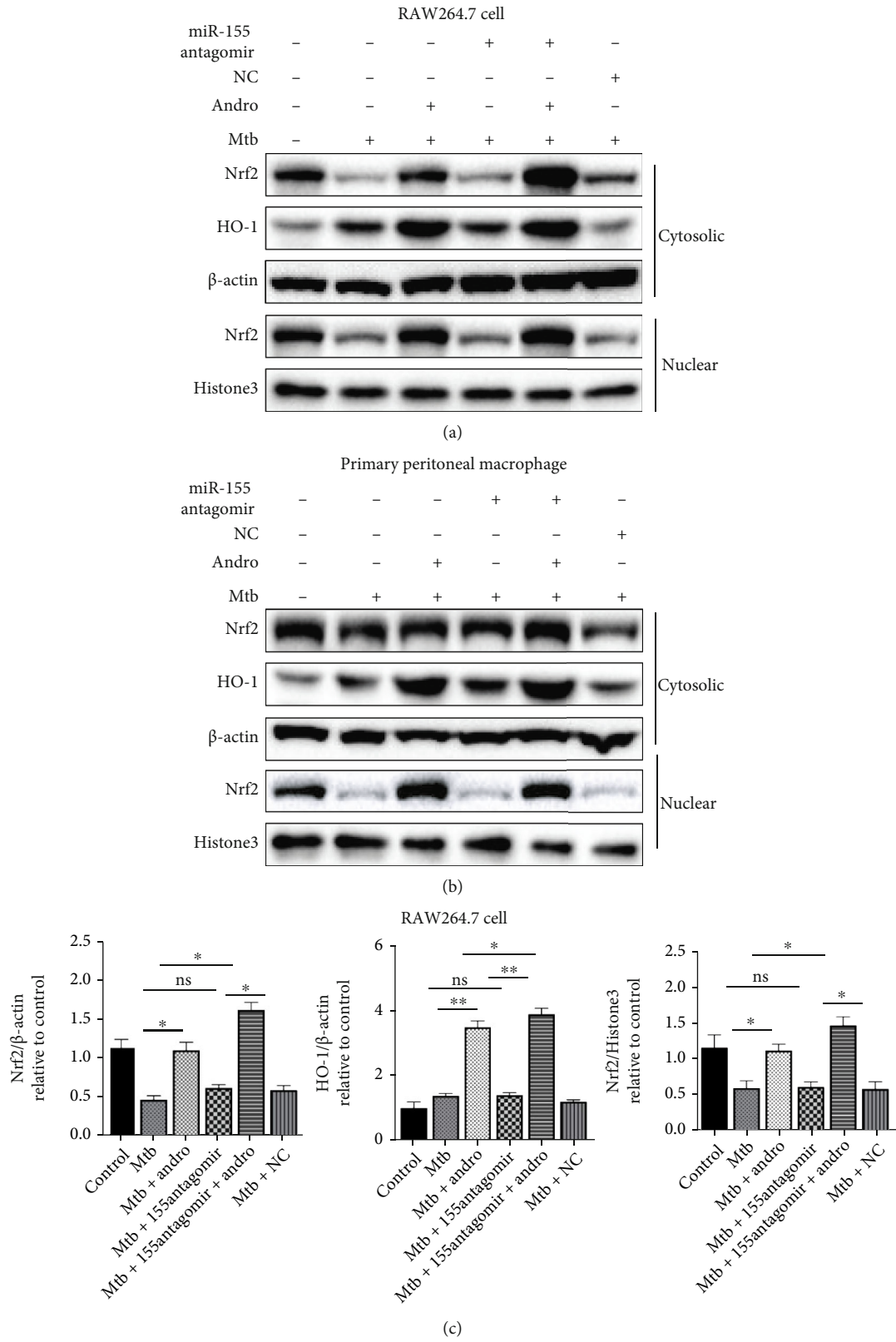


FIGURE 7: Continued.

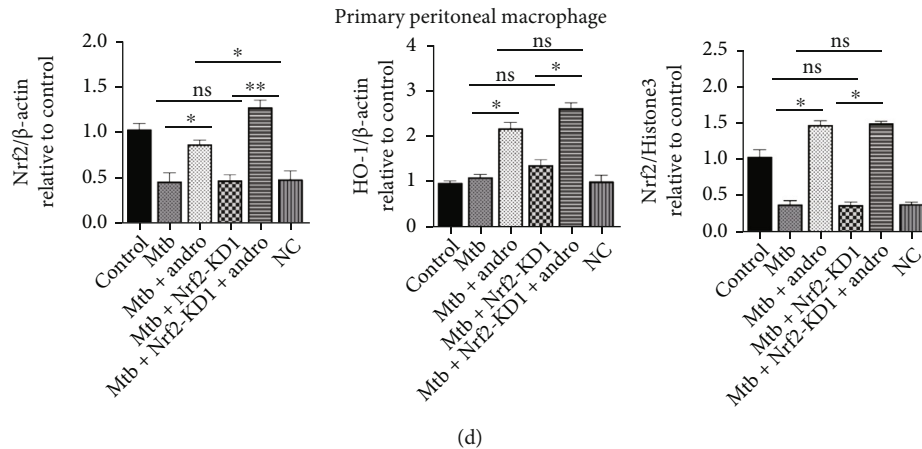


FIGURE 7: miR-155-5p antagonist upregulates the expression of Nrf2 and HO-1 in Mtb-infected macrophages. (a, c) The expressions of Nrf2 and HO-1 were analyzed by western blotting after miR-155-5p antagonist treatment in RAW264.7 cells. (b, d) The levels of Nrf2 and HO-1 proteins were assessed by western blotting after miR-155-5p antagonist treatment in primary peritoneal macrophage cells. Data are shown as mean \pm SD of three independent experiments. NC: negative control. * $p < 0.05$, ** $p < 0.01$. ns: nonsignificant.

have demonstrated that there are many miRNAs implicated in excessive inflammatory response and pyroptosis [46–49], including miR-155-5p [18]. Some of these studies have shown that miR-155-5p promotes macrophage pyroptosis via regulation of the NLRP3 inflammasome [50]. Thus, we hypothesized that miR-155-5p may be a key target in the Andro-mediated inhibition of pyroptosis in Mtb-infected macrophages. Thus, we decided to evaluate the expression of miR-155-5p in response to both Mtb and Andro treatment using RT-PCR. These evaluations showed that miR-155-5p was upregulated in response to increasing time of infection and that this was significantly reduced following the addition of Andro, in both macrophage models (Figures 2(a) and 2(b)).

MiR-155HG is a precursor of miR-155-5p, which also acts as a long noncoding RNA (lncRNA) regulating M1/M2 macrophage polarization in chronic obstructive pulmonary disease [51–53]. We also evaluated the expression of miR-155HG under these treatment conditions, with these experiments producing similar results to miR-155-5p. Mtb infection increases the expression of miR-155HG, whereas Andro treatment reduces its expression in response to Mtb (Figures 2(a) and 2(b)).

To further confirm whether Andro inhibits pyroptosis in Mtb-infected macrophages through the downregulation of miR-155-5p, we assessed GSDMD-N and IL-1 β using miR-155-5p mimic, inhibitor, and antagonist.

Interestingly, the overexpression of intracellular miR-155-5p increased Mtb-induced IL-1 β expression and acted as an antagonist of the Andro-mediated downregulation of this cytokine, suggesting that an increase in miR-155-5p expression may exacerbate inflammation and impair the anti-inflammatory effects of Andro (Figures 2(c) and 2(d)). Similarly, GSDMD-N in Mtb-infected macrophages was also slightly upregulated in response to treatment with miR-155-5p mimic, while the anti-inflammatory effects of Andro were inhibited by its overexpression, suggesting that miR-155-5p expression promotes pyroptosis and Andro treatment inhibits it (Figures 3(a) and 3(b)). Furthermore, both miR-

155-5p inhibitor and antagonist produced similar effects to the Andro treatment, including a reduction in IL-1 β (Figures 2(c) and 2(d)) and GSDMD-N (Figures 3(c)–3(f)), suggesting an overall decrease in pyroptosis. Taken together, these results suggest that Andro inhibits pyroptosis in Mtb-infected macrophages via the downregulation of miR-155-5p, which may reduce the overall inflammatory response and pyroptosis in Mtb-infected macrophages.

Notably, IL-1 β was further downregulated, and infected cells were treated with both miR-155-5p inhibitor or antagonist and Andro, suggesting that there are likely other mechanisms underlying Andro-mediated reductions in the inflammatory response. However, this phenomenon was not observed in evaluations of GSDMD-N (Figures 3(c)–3(f)).

3.3. Andro Activates the Nrf2/HO-1 Pathway through Inhibition of miR-155-5p Expression in Mtb-Infected Macrophages. miRNAs generally work by binding to and regulating the expression of downstream target genes. Based on this, we evaluated the mechanism underlying these anti-inflammatory effects by identifying and evaluating the potential targets of miR-155-5p. We used TargetScan (<http://www.targetscan.org>) and found that the 3'-UTR of mouse Nrf2 mRNA as a putative target site for miR-155-5p (Figures 4(a) and 4(b)).

Studies have shown that Andro can inhibit inflammation by regulating the expression of Nrf2 [54, 55]. To determine whether Andro has an effect on Nrf2 and its downstream antioxidant genes in Mtb infection model, the mRNA of Nrf2, HO-1, and NQO-1 (HO-1 and NQO-1 are the downstream antioxidant genes of Nrf2) was detected in Mtb group and Andro group.

The results suggested that Andro significantly upregulated the expressions of these antioxidant genes (Figures 4(c) and 4(d)). Generally, accumulation of Nrf2 and its translocation into the nucleus can promote the expression of HO-1 and NQO-1. Thus, we also analyzed the protein levels of Nrf2 in

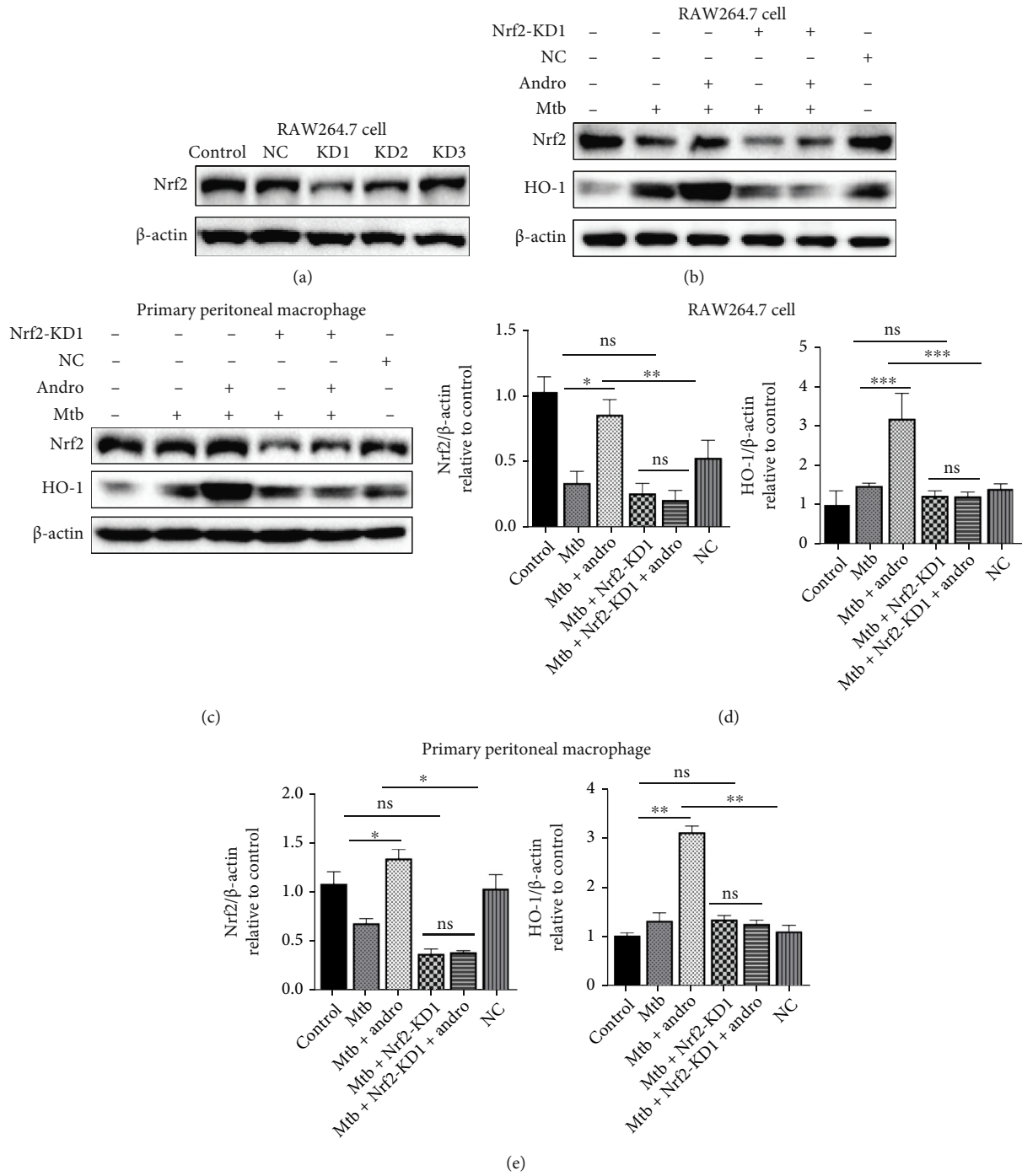


FIGURE 8: Continued.

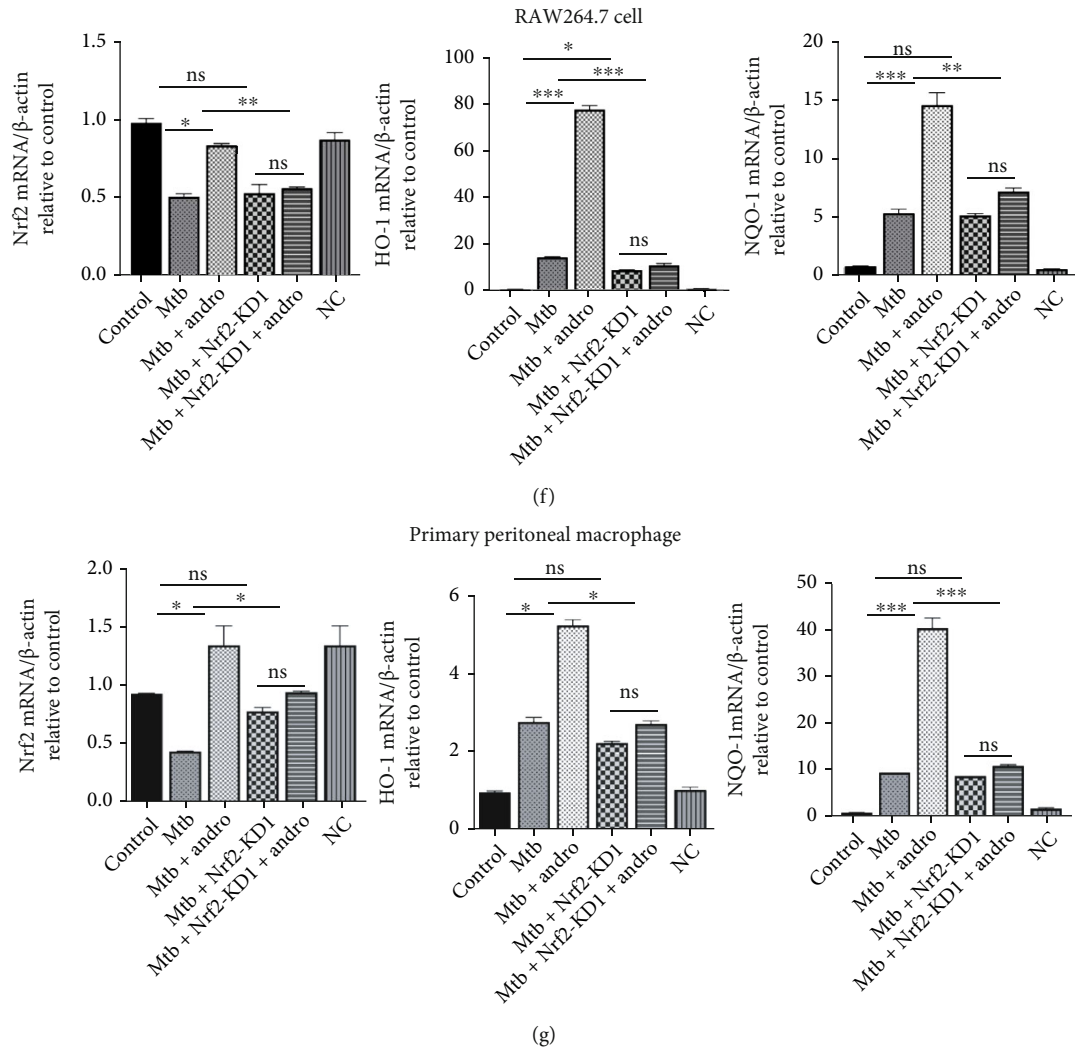


FIGURE 8: siNrf2 can inhibit the antioxidant effect of Andro in macrophages infected with Mtb. (a) Transfection efficiency of siRNAs was measured by western blotting analysis in RAW264.7 cells. (b, d) The levels of Nrf2 and HO-1 proteins were measured by western blotting after siNrf2 in RAW264.7 cells. (c, e) The levels of Nrf2 and HO-1 proteins were measured by western blotting after siNrf2 in primary peritoneal macrophage cells. (f, g) The levels of Nrf2, HO-1, and NQO-1 mRNAs were measured by RT-PCR after siNrf2 in RAW264.7 cells and primary peritoneal macrophage cells, respectively. Data are shown as mean \pm SD of three independent experiments. NC: negative control. * $p < 0.05$, ** $p < 0.01$, *** $p < 0.001$. ns: nonsignificant.

the cytoplasm and nucleus of these cells and demonstrated that Andro treatment induced nuclear translocation of Nrf2 and increased the expression of HO-1 in the cytoplasm (Figures 4(e) and 4(f)).

To determine whether Nrf2 is regulated by miR-155-5p, we assessed the levels of Nrf2 in the cytoplasm and nucleus of cells treated with miR-155-5p mimic. In the miR-155-5p mimic group, the mimic weakened the translocation of Nrf2, and the level of HO-1 induced by Andro (Figures 5(a)–5(d)) revealed that miR-155-5p is a mediator of Nrf2 and HO-1.

Then, these observations were validated by transfecting miR-155-5p inhibitor or antagomir into Mtb-infected macrophages and evaluating Nrf2 and HO-1 expression. The results revealed that the inhibition of miR-155-5p resulted in little change in the translocation of Nrf2 but with a signif-

icant increase in cytoplasmic HO-1. However, when miR-155-5p inhibitor-treated cells were also exposed to Andro, we noted an increased translocation of Nrf2 compared with Andro alone, although these outcomes were more obvious in RAW264.7 cells (Figures 6(a)–6(d) and 7(a)–(d)). These findings reveal that Andro activates and subsequently promotes Nrf2 translocation into the nucleus by inhibiting miR-155-5p.

3.4. Andro Ameliorates Pyroptosis by Activating Nrf2/HO-1 Pathway in Mtb-Infected Macrophages. Our data support the hypothesis that Andro inhibits miR-155-5p expression activating the Nrf2/HO-1 pathway and that this compound ameliorates pyroptosis in Mtb-infected macrophages. However, it is not clear whether Andro inhibits pyroptosis via activation of the Nrf2/HO-1 pathway. Here, we used siNrf2

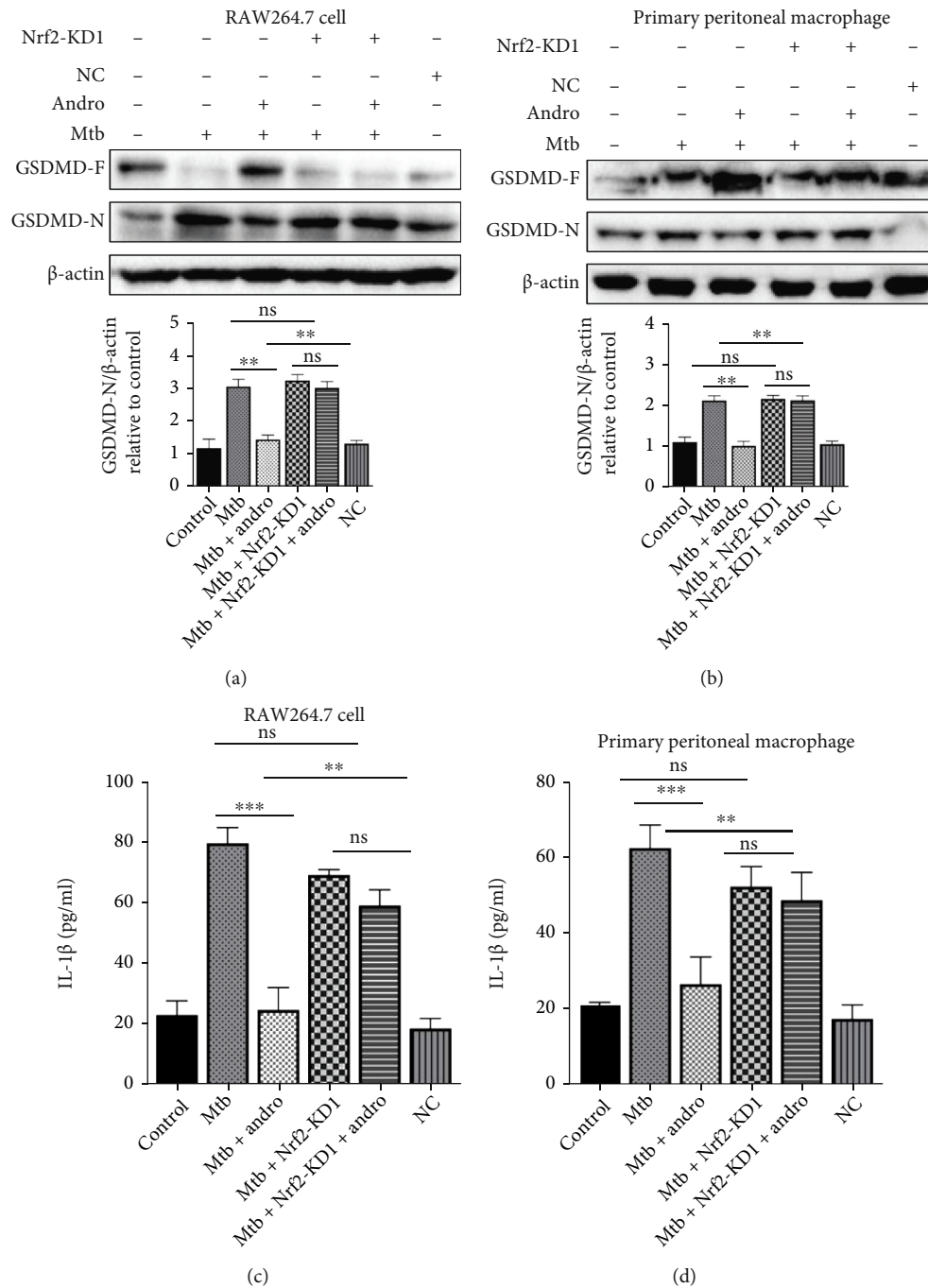


FIGURE 9: siNrf2 can eliminate the effect of Andro on inhibiting pyroptosis in Mtb-infected macrophages. (a, b) The expressions of GSDMD-N were analyzed by western blotting after siNrf2 in RAW264.7 cells and primary peritoneal macrophage cells, respectively. (c, d) Release of IL- β was assessed by ELISA measurement after siNrf2 in RAW264.7 cells and primary peritoneal macrophage cells, respectively. Data are shown as mean \pm SD of three independent experiments. NC: negative control. ** $p < 0.01$, *** $p < 0.001$. ns: nonsignificant.

to knock down Nrf2 expression and then assessed the level of GSDMD-N. We used three siRNAs to knock down Nrf2 and noted that KD1 had the best effect (Figure 8(a)). Thus, we used KD1 as the siNrf2 in our downstream evaluations. Our results demonstrated that HO-1 was decreased following treatment with siNrf2 and that this could not be rescued by the addition of Andro (Figures 8(b)–8(e)).

Similar results also were found in mRNAs levels suggesting that Andro-mediated inhibition of oxidative stress depends on Nrf2 (Figures 8(f) and 8(g)). In order to verify whether Andro treatment suppressed pyroptosis in Mtb-infected macrophages, we evaluated GSDMD-N production following the addition of siNrf2. These results demonstrated that when Nrf2 was knocked down, GSDMD-N was upregulated

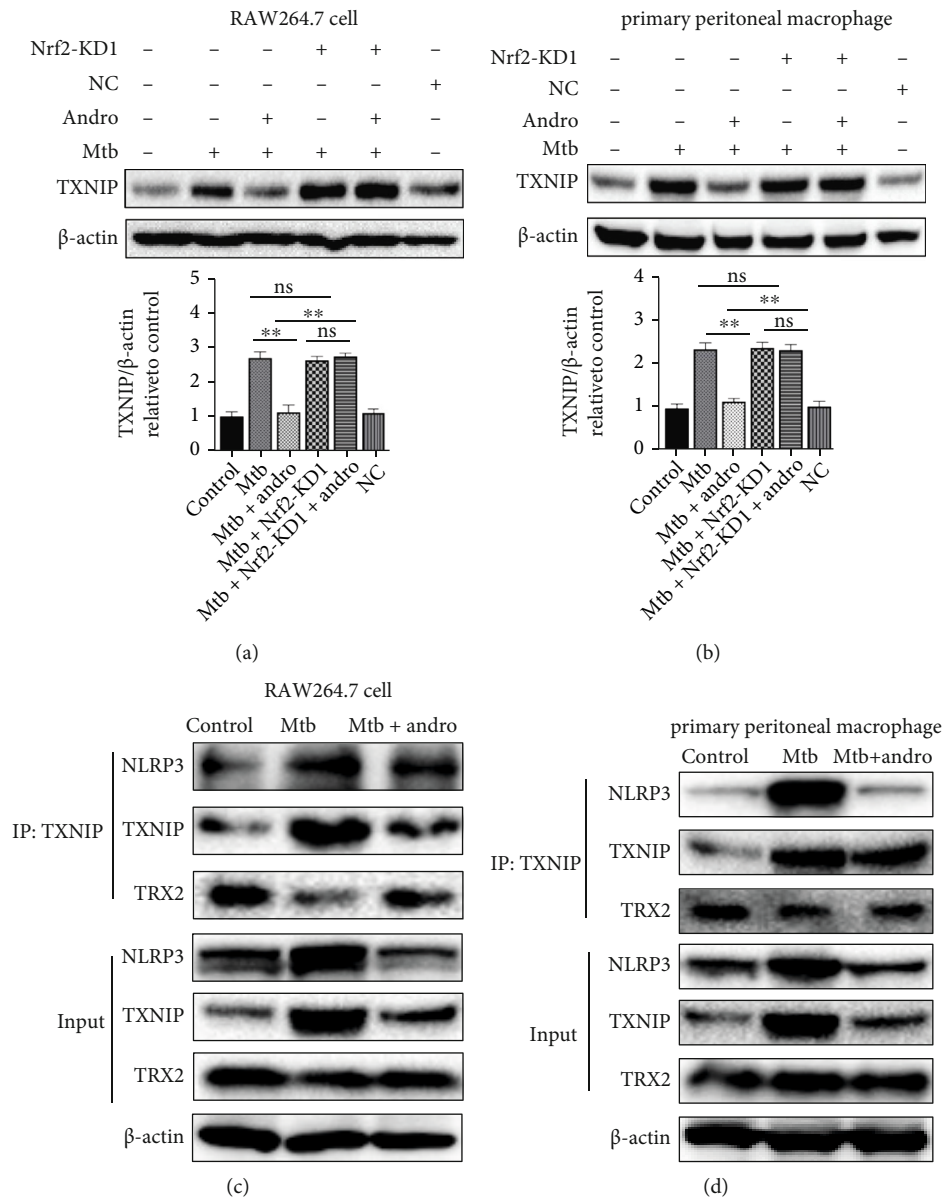
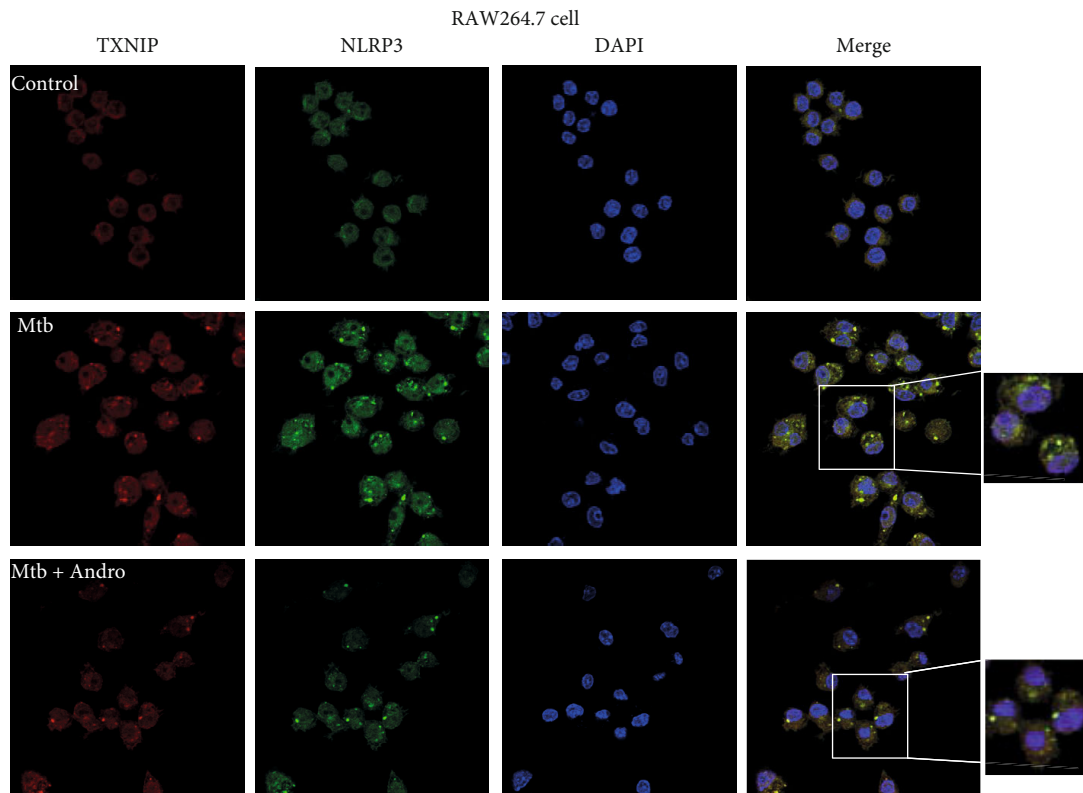


FIGURE 10: siNrf2 could abolish the effect of Andro on inhibiting the NLRP3 inflammasome activation. (a, b) Levels of TXNIP protein were analyzed by western blotting after siNrf2 in RAW264.7 cells and primary peritoneal macrophage cells, respectively. (c, d) TXNIP or NLRP3 immunoprecipitated from RAW264.7 cells and primary peritoneal macrophage cells were immunoblotted for TXNIP and re-blotted for NLRP3, TXNIP, and TRX2, respectively. Data are shown as mean ± SD of three independent experiments. NC: negative control. * $p < 0.05$, ** $p < 0.01$. ns: nonsignificant.

in Mtb-infected macrophages and that this increase could not be reversed by Andro treatment (Figures 9(a) and 9(b)). Similar results were observed in IL-1 β level (Figures 9(c) and 9(d)). These results revealed that Andro inhibits pyroptosis in Mtb-infected macrophages through the activation of the Nrf2/HO-1 pathway.

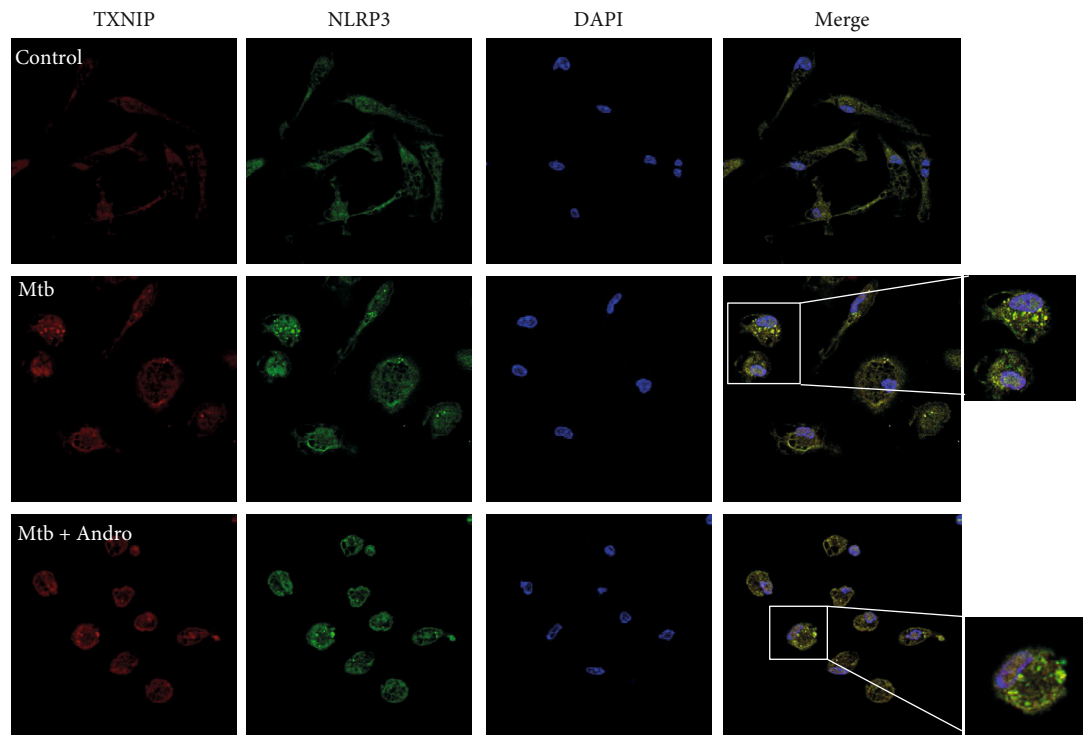
3.5. Andro Inhibits Pyroptosis through Its Interactions with the Nrf2/TXNIP/NLRP3 Axis in Mtb-Infected Macrophages. To further study the underlying connections between Nrf2 and the NLRP3 inflammasome, we focused on the effects of these treatments on thioredoxin interacting protein (TXNIP). TXNIP is a member of the thioredoxin (TRX) sys-

tem and an endogenous regulator of redox/glucose-induced stress and inflammation [56, 57]. TXNIP usually combines with TRX2, but excessive ROS can induce their dissociation allowing free TXNIP to combine with NLRP3 activating it and inducing an excessive inflammatory response [56, 58, 59]. We then investigated whether TXNIP acts as a mediator between Nrf2 and NLRP3 using siNrf2. The results demonstrated that TXNIP was upregulated in Mtb-infected macrophages but was significantly reduced in Andro-treated cells, but that this reduction was inhibited by the addition of siNrf2 (Figures 10(a) and 10(b)). These results indicated that Andro suppresses the expression of TXNIP and that this is dependent on Nrf2.



(a)

primary peritoneal macrophage



(b)

FIGURE 11: Andro reduces the colocalization of TXNIP and NLRP3 in Mtb-infected macrophages. (a, b) Confocal microscopy of RAW264.7 cells and primary peritoneal macrophage cells with different treatments immunostained with anti-TXNIP (red), anti-NLRP3 (green), and DAPI (blue), respectively. Data are shown as mean \pm SD of three independent experiments.

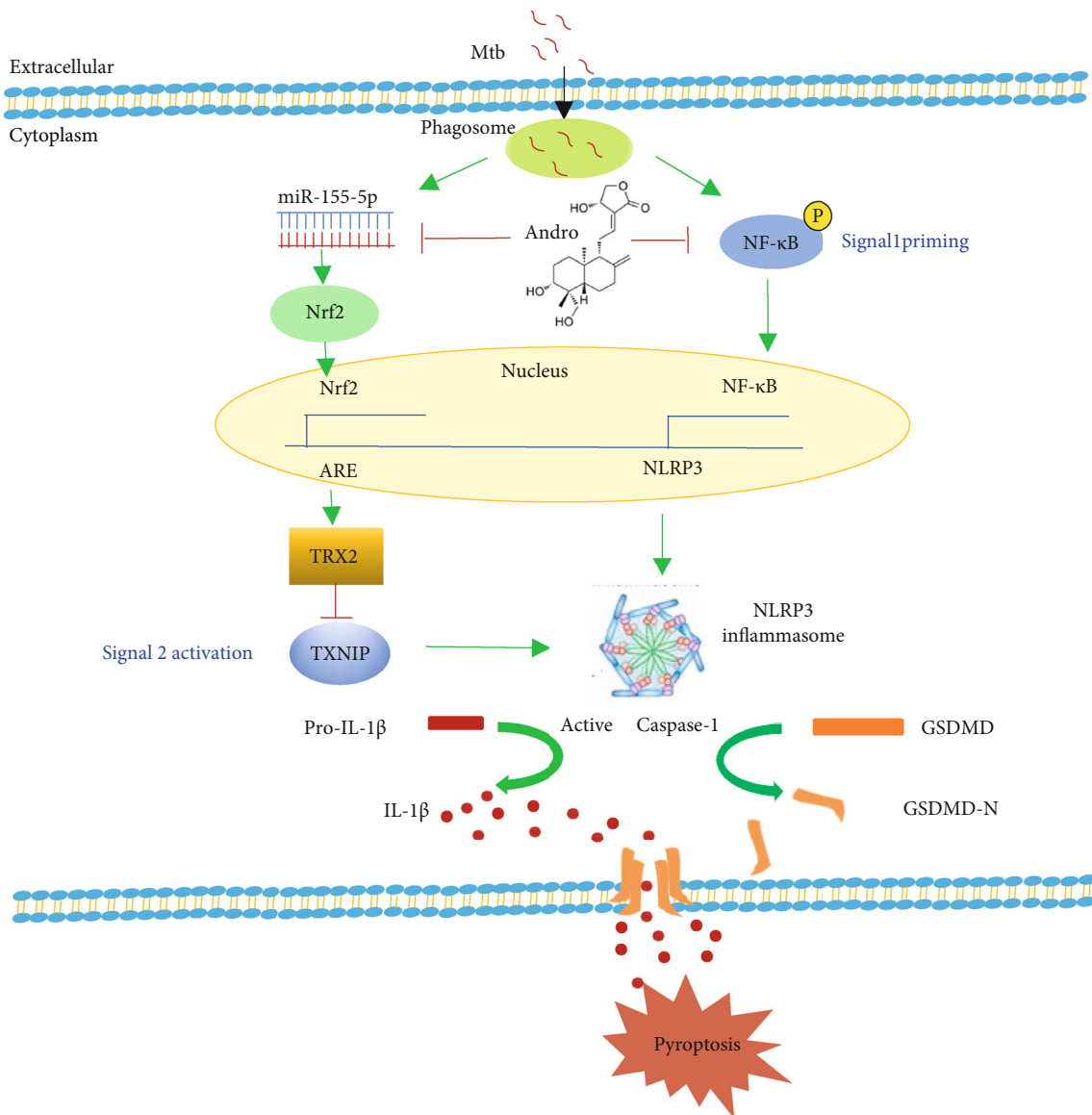


FIGURE 12: Illustration of Andro suppressing pyroptosis in Mtb-infected macrophages. Previous work has demonstrated that Andro inhibits activation of NLRP3 inflammasome through NF- κ B pathway [42]. Here, we revealed that Andro also attenuates pyroptosis in Mtb-infected macrophages via the miR-155-5p/Nrf2 axis.

To define whether the effect of Andro on the NLRP3 inflammasome was mediated by the upregulation of Nrf2, coimmunoprecipitation was used to analyze the interaction between TXNIP and TRX2. The interaction was reduced following Mtb infection and was restored following the addition of Andro (Figures 10(c) and 10(d)). We then investigated the interaction between TXNIP and NLRP3 by coimmunoprecipitation and immunofluorescence to determine whether the increased TXNIP expression could lead to NLRP3 inflammasome activation. These results showed that the interaction between TXNIP and the NLRP3 inflammasome increased in Mtb-infected macrophages and that the addition of Andro attenuated this interaction (Figures 10(c) and 10(d)). Confocal imaging also demonstrated that Mtb infection increased the colocalization of NLRP3 and TXNIP, while Andro treatment significantly downregulated their expressions and

reduced their colocalization (Figure 11). These results revealed that Andro significantly attenuates pyroptosis via its interactions with the Nrf2/TXNIP/NLRP3 axis in Mtb-infected macrophages.

4. Discussion

Current research suggests that the primary cause of death in most TB patients is not their bacterial infection, but rather the tissue damage resulting from their excessive inflammatory response to this infection. Therefore, effective treatment of TB patients is likely to require both elimination of the Mtb and prevention of this inflammatory response. HDT is based on the concept of balancing the host's immune system and may offer a novel approach for the discovery of new anti-TB therapies.

Pyroptosis is a recently described type of cell death, which, unlike apoptosis, may induce excessive inflammatory responses [60]. Studies have reported that Mtb infection can induce macrophage pyroptosis, which in turn induces the release of proinflammatory factors and aggravates tissue damage. In addition, pyroptosis in Mtb-infected macrophages can result in the systemic release of Mtb and increased infection [10].

Andro, an active ingredient extracted from *Andrographis paniculata*, has been reported to have anti-inflammatory and antitumor effects [61, 62]. Our previous study found that this compound can suppress NLRP3 inflammasome activation through the NF- κ B signaling pathway, thereby inhibiting the excessive inflammatory response induced by Mtb infection [42]. Mtb infection can also induce pyroptosis and excessive inflammatory responses in macrophages [63], and Andro has a known anti-inflammatory effect. Thus, we hypothesized that Andro might be able to prevent excessive inflammatory responses by inhibiting the pyroptosis in Mtb-infected macrophages. Here, we used western blotting to assess GSDMD-N and PI staining to prove that Andro treatment inhibits pyroptosis in Mtb-infected macrophages. However, due to limited conditions, we were unable to directly observe this phenomenon using electron microscopy. We hope to address this aspect in the future.

The occurrence of pyroptosis is accompanied by many factors, including the production of pro-inflammatory miRNAs and the activation of the inflammasomes [64, 65]. Based on this, we also analyzed these factors to identify the specific mechanism underlying Andro-mediated inhibition of pyroptosis. The previous studies have revealed that miR-155-5p has a strong proinflammatory effect in Mtb infection [66]. In the present study, we evaluated its association with pyroptosis. These results demonstrated that Andro treatment inhibits macrophage pyroptosis by downregulating miR-155-5p.

Given that most miRNAs could exert their effect by promoting the degradation or inhibiting the translation of their target genes, we identified the target genes for miR-155-5p. Our evaluations identified the antioxidant gene Nrf2 as one of the targets of miR-155-5p, and Nrf2 activation is also a known factor in the inhibition of excessive inflammation [34, 36, 67], we evaluated its effects on pyroptosis and whether this might be the mechanism underlying Andro-mediated inhibition of excessive inflammation. Our results revealed that Nrf2 is the target gene of miR-155-5p, and that Andro treatment upregulated the expression of Nrf2 by downregulating miR-155-5p, thereby inhibiting pyroptosis in Mtb-infected macrophages.

After activation, Nrf2 is translocated to the nucleus where it promotes the expression of several antioxidant genes, including TRX2, HO-1, and NQO-1 [68, 69]. Under normal conditions, TRX2 combines with TXNIP, but oxidative stress induces their dissociation and allows free TXNIP to combine with the NLRP3 inflammasome, activating the latter and eventually promoting the inflammatory response [70]. Studies have shown that activation of the NLRP3 inflammasome induces the release of various pro-inflammatory factors, which eventually leads to pyroptosis [71]. Our results dem-

onstrated that Andro treatment inhibits NLRP3 inflammasome activation by suppressing the interaction between TXNIP and NLRP3. Thus, our data revealed that Andro likely attenuates pyroptosis in Mtb-infected macrophages via the miR-155-5p/Nrf2 axis (Figure 12).

Of course, there are still some shortcomings in this study. Firstly, we did not use Andro alone to treat normal macrophages to evaluate whether the drug had an effect on factors such as Nrf2, cytokines, and miRNAs. Therefore, we will pay attention to these phenomena in future studies. Besides, we used H37Ra to infect RAW264.7 cell and mouse primary peritoneal macrophages as an in vitro infection model. H37Ra strain is an avirulent strain and has a similar genetic background to H37Rv strain, but it is easier to operate and safer [72, 73]. In the future study, we will evaluate the potential of Andro as an adjuvant therapy against TB in animal models of H37Rv infection.

Data Availability

The data used to support the findings of this study are available from the corresponding author upon request.

Conflicts of Interest

The authors declare that they have no conflicts of interest.

Authors' Contributions

XJ and YZ conceived and designed the experiments. YF, JS, FL, and HZ perform the experiments. YF and JS analyzed the data. YF and XJ wrote the paper. All authors have read and approved the final manuscript.

Acknowledgments

This study was supported by the Research on the Material Basis and Mechanism of Qingfei Paidu Decoction in the Treatment of Coronavirus Disease (2021YFE0200900), the National Natural Science Foundation of China (81873069 and 82073901), and the Shanghai Science and Technology Planning Program (21DZ2271000).

References

- [1] M. Schito, G. B. Migliori, H. A. Fletcher et al., "Perspectives on advances in tuberculosis diagnostics, drugs, and vaccines," *Clinical Infectious Diseases*, vol. 61, Supplement 3, pp. S102–S118, 2015.
- [2] L. C. K. Bell and M. Noursadeghi, "Pathogenesis of HIV-1 and Mycobacterium tuberculosis co-infection," *Nature Reviews. Microbiology*, vol. 16, no. 2, pp. 80–90, 2018.
- [3] T. J. Scriba, A. K. Coussens, and H. A. Fletcher, "Human immunology of tuberculosis," *Microbiology Spectrum*, vol. 5, no. 1, 2017.
- [4] Y. Wang, H. Zhang, Q. Chen et al., "TNF- α /HMGB1 inflammation signalling pathway regulates pyroptosis during liver failure and acute kidney injury," *Cell Proliferation*, vol. 53, no. 6, article e12829, 2020.

- [5] S. H. E. Kaufmann, A. Dorhoi, R. S. Hotchkiss, and R. Bartenschlager, "Host-directed therapies for bacterial and viral infections," *Nature Reviews. Drug Discovery*, vol. 17, no. 1, pp. 35–56, 2018.
- [6] Z. Hmama, S. Peña-Díaz, S. Joseph, and Y. Av-Gay, "Immuno-evasion and immunosuppression of the macrophage by *Mycobacterium tuberculosis*," *Immunological Reviews*, vol. 264, no. 1, pp. 220–232, 2015.
- [7] S. Tiberi, N. du Plessis, G. Walzl et al., "Tuberculosis: progress and advances in development of new drugs, treatment regimens, and host-directed therapies," *The Lancet Infectious Diseases*, vol. 18, no. 7, pp. e183–e198, 2018.
- [8] R. Tang, J. Xu, B. Zhang et al., "Ferroptosis, necroptosis, and pyroptosis in anticancer immunity," *Journal of Hematology & Oncology*, vol. 13, no. 1, p. 110, 2020.
- [9] K. S. Beckwith, M. S. Beckwith, S. Ullmann et al., "Plasma membrane damage causes NLRP3 activation and pyroptosis during *Mycobacterium tuberculosis* infection," *Nature Communications*, vol. 11, no. 1, p. 2270, 2020.
- [10] Z. Qu, J. Zhou, Y. Zhou et al., "Mycobacterial EST12 activates a RACK1-NLRP3-gasdermin D pyroptosis-IL-1 β immune pathway," *Science Advances*, vol. 6, no. 43, 2020.
- [11] A. Welin, D. Eklund, O. Stendahl, and M. Lerm, "Human macrophages infected with a high burden of ESAT-6-expressing *M. tuberculosis* undergo caspase-1- and cathepsin B-independent necrosis," *PLoS One*, vol. 6, no. 5, article e20302, 2011.
- [12] K. Saliminejad, H. R. Khorram Khorshid, S. Soleymani Fard, and S. H. Ghaffari, "An overview of microRNAs: biology, functions, therapeutics, and analysis methods," *Journal of Cellular Physiology*, vol. 234, no. 5, pp. 5451–5465, 2019.
- [13] Y. Sun, Q. Li, H. Gui et al., "MicroRNA-124 mediates the cholinergic anti-inflammatory action through inhibiting the production of pro-inflammatory cytokines," *Cell Research*, vol. 23, no. 11, pp. 1270–1283, 2013.
- [14] W. Xiaoyan, E. M. A. Pais, L. Lan et al., "MicroRNA-155: a novel armamentarium against inflammatory diseases," *Inflammation*, vol. 40, no. 2, pp. 708–716, 2017.
- [15] K. Fisher and J. Lin, "MicroRNA in inflammatory bowel disease: translational research and clinical implication," *World Journal of Gastroenterology*, vol. 21, no. 43, pp. 12274–12282, 2015.
- [16] K. Jiang, J. Yang, S. Guo, G. Zhao, H. Wu, and G. Deng, "Peripheral circulating exosome-mediated delivery of miR-155 as a novel mechanism for acute lung inflammation," *Molecular Therapy*, vol. 27, no. 10, pp. 1758–1771, 2019.
- [17] C. Wang, C. Zhang, L. Liu et al., "Macrophage-derived miR-155-containing exosomes suppress fibroblast proliferation and promote fibroblast inflammation during cardiac injury," *Molecular Therapy*, vol. 25, no. 1, pp. 192–204, 2017.
- [18] A. C. Rothchild, J. R. Sissons, S. Shafiani et al., "MiR-155-regulated molecular network orchestrates cell fate in the innate and adaptive immune response to *Mycobacterium tuberculosis*," *Proceedings of the National Academy of Sciences of the United States of America*, vol. 113, no. 41, pp. E6172–E6181, 2016.
- [19] D. S. Ghorpade, R. Leyland, M. Kurowska-Stolarska, S. A. Patil, and K. N. Balaji, "MicroRNA-155 is required for *Mycobacterium bovis* BCG-mediated apoptosis of macrophages," *Molecular and Cellular Biology*, vol. 32, no. 12, pp. 2239–2253, 2012.
- [20] E. Tsitsiou and M. A. Lindsay, "microRNAs and the immune response," *Current Opinion in Pharmacology*, vol. 9, no. 4, pp. 514–520, 2009.
- [21] E. Tili, J. J. Michaille, A. Cimino et al., "Modulation of miR-155 and miR-125b levels following lipopolysaccharide/TNF-alpha stimulation and their possible roles in regulating the response to endotoxin shock," *Journal of Immunology*, vol. 179, no. 8, pp. 5082–5089, 2007.
- [22] X. Zhou, T. Yan, C. Huang et al., "Melanoma cell-secreted exosomal miR-155-5p induce proangiogenic switch of cancer-associated fibroblasts via SOCS1/JAK2/STAT3 signaling pathway," *Journal of Experimental & Clinical Cancer Research*, vol. 37, no. 1, p. 242, 2018.
- [23] Y. Wang, Z. J. Zheng, Y. J. Jia, Y. L. Yang, and Y. M. Xue, "Role of p53/miR-155-5p/sirt1 loop in renal tubular injury of diabetic kidney disease," *Journal of Translational Medicine*, vol. 16, no. 1, p. 146, 2018.
- [24] M. Wu, Q. Duan, X. Liu et al., "MiR-155-5p promotes oral cancer progression by targeting chromatin remodeling gene ARID2," *Biomedicine & Pharmacotherapy*, vol. 122, article 109696, 2020.
- [25] L. Xu, H. Ji, Y. Jiang et al., "Exosomes derived from CircAkap7-modified adipose-derived mesenchymal stem cells protect against cerebral ischemic injury," *Frontiers in Cell and Development Biology*, vol. 8, article 569977, 2020.
- [26] P. Y. Lee, C. D. Platt, S. Weeks et al., "Immune dysregulation and multisystem inflammatory syndrome in children (MIS-C) in individuals with haploinsufficiency of SOCS1," *The Journal of Allergy and Clinical Immunology*, vol. 146, no. 5, pp. 1194–1200.e1, 2020.
- [27] K. Nakamura, M. Zhang, S. Kageyama et al., "Macrophage heme oxygenase-1-SIRT1-p53 axis regulates sterile inflammation in liver ischemia-reperfusion injury," *Journal of Hepatology*, vol. 67, no. 6, pp. 1232–1242, 2017.
- [28] Y. Wang, T. Zhao, Y. Deng et al., "Genipin ameliorates carbon tetrachloride-induced liver injury in mice via the concomitant inhibition of inflammation and induction of autophagy," *Oxidative Medicine and Cellular Longevity*, vol. 2019, Article ID 3729051, 12 pages, 2019.
- [29] E. H. Kobayashi, T. Suzuki, R. Funayama et al., "Nrf2 suppresses macrophage inflammatory response by blocking proinflammatory cytokine transcription," *Nature Communications*, vol. 7, no. 1, article 11624, 2016.
- [30] X. Sun, Z. Ou, R. Chen et al., "Activation of the p62-Keap1-NRF2 pathway protects against ferroptosis in hepatocellular carcinoma cells," *Hepatology*, vol. 63, no. 1, pp. 173–184, 2016.
- [31] J. Li, H. Wang, Z. Zheng et al., "Mkp-1 cross-talks with Nrf2/Ho-1 pathway protecting against intestinal inflammation," *Free Radical Biology & Medicine*, vol. 124, pp. 541–549, 2018.
- [32] A. Loboda, M. Damulewicz, E. Pyza, A. Jozkowicz, and J. Dulak, "Role of Nrf2/HO-1 system in development, oxidative stress response and diseases: an evolutionarily conserved mechanism," *Cellular and Molecular Life Sciences*, vol. 73, no. 17, pp. 3221–3247, 2016.
- [33] M. Ge, W. Yao, D. Yuan et al., "Brg1-mediated Nrf2/HO-1 pathway activation alleviates hepatic ischemia-reperfusion injury," *Cell Death & Disease*, vol. 8, no. 6, article e2841, 2017.
- [34] C. Diao, Z. Chen, T. Qiu et al., "Inhibition of PRMT5 attenuates oxidative stress-induced pyroptosis via activation of the Nrf2/HO-1 signal pathway in a mouse model of renal

- ischemia-reperfusion injury,” *Oxidative Medicine and Cellular Longevity*, vol. 2019, Article ID 2345658, 18 pages, 2019.
- [35] C. Huang, C. Zhang, P. Yang et al., “Eldecalcitol inhibits LPS-induced NLRP3 inflammasome-dependent pyroptosis in human gingival fibroblasts by activating the Nrf2/HO-1 signaling pathway,” *Drug Design, Development and Therapy*, vol. 14, pp. 4901–4913, 2020.
- [36] Y. Lin, T. Luo, A. Weng et al., “Gallic acid alleviates gouty arthritis by inhibiting NLRP3 inflammasome activation and pyroptosis through enhancing Nrf2 signaling,” *Frontiers in Immunology*, vol. 11, article 580593, 2020.
- [37] J. Gao, S. Peng, X. Shan et al., “Inhibition of AIM2 inflammasome-mediated pyroptosis by andrographolide contributes to amelioration of radiation-induced lung inflammation and fibrosis,” *Cell Death & Disease*, vol. 10, no. 12, p. 957, 2019.
- [38] M. T. Islam, E. S. Ali, S. J. Uddin et al., “Andrographolide, a diterpene lactone from *Andrographis paniculata* and its therapeutic promises in cancer,” *Cancer Letters*, vol. 420, pp. 129–145, 2018.
- [39] F. Li, E. M. Lee, X. Sun, D. Wang, H. Tang, and G. C. Zhou, “Design, synthesis and discovery of andrographolide derivatives against Zika virus infection,” *European Journal of Medicinal Chemistry*, vol. 187, article 111925, 2020.
- [40] W. S. D. Tan, W. Liao, H. Y. Peh et al., “Andrographolide simultaneously augments Nrf2 antioxidant defense and facilitates autophagic flux blockade in cigarette smoke-exposed human bronchial epithelial cells,” *Toxicology and Applied Pharmacology*, vol. 360, pp. 120–130, 2018.
- [41] S. Y. Wong, M. G. K. Tan, P. T. H. Wong, D. R. Herr, and M. K. P. Lai, “Andrographolide induces Nrf2 and heme oxygenase 1 in astrocytes by activating p38 MAPK and ERK,” *Journal of Neuroinflammation*, vol. 13, no. 1, p. 251, 2016.
- [42] W. He, J. Sun, Q. Zhang et al., “Andrographolide exerts anti-inflammatory effects in *Mycobacterium tuberculosis*-infected macrophages by regulating the Notch1/Akt/NF- κ B axis,” *Journal of Leukocyte Biology*, vol. 108, no. 6, pp. 1747–1764, 2020.
- [43] Y. Fu, J. Shen, Y. Li et al., “Inhibition of the PERK/TXNIP/NLRP3 axis by baicalin reduces NLRP3 inflammasome-mediated pyroptosis in macrophages infected with *Mycobacterium tuberculosis*,” *Mediators of Inflammation*, vol. 2021, Article ID 1805147, 15 pages, 2021.
- [44] Q. Zhang, J. Sun, Y. Wang et al., “Antimycobacterial and anti-inflammatory mechanisms of baicalin via induced autophagy in macrophages infected with *Mycobacterium tuberculosis*,” *Frontiers in Microbiology*, vol. 8, p. 2142, 2017.
- [45] S. Xu, H. Chen, H. Ni, and Q. Dai, “Targeting HDAC6 attenuates nicotine-induced macrophage pyroptosis via NF- κ B/NLRP3 pathway,” *Atherosclerosis*, vol. 317, pp. 1–9, 2021.
- [46] S. M. Man, R. Karki, and T. D. Kanneganti, “Molecular mechanisms and functions of pyroptosis, inflammatory caspases and inflammasomes in infectious diseases,” *Immunological Reviews*, vol. 277, no. 1, pp. 61–75, 2017.
- [47] C. Palma, C. la Rocca, V. Gigantino et al., “Caloric restriction promotes immunometabolic reprogramming leading to protection from tuberculosis,” *Cell Metabolism*, vol. 33, no. 2, pp. 300–318.e12, 2021.
- [48] S. Nair, J. P. Huynh, V. Lampropoulou et al., “Irg1 expression in myeloid cells prevents immunopathology during *M. tuberculosis* infection,” *The Journal of Experimental Medicine*, vol. 215, no. 4, pp. 1035–1045, 2018.
- [49] Q. Chai, X. Wang, L. Qiang et al., “A *Mycobacterium tuberculosis* surface protein recruits ubiquitin to trigger host xenophagy,” *Nature Communications*, vol. 10, no. 1, p. 1973, 2019.
- [50] C. Li, W. Yin, N. Yu et al., “miR-155 promotes macrophage pyroptosis induced by *Porphyromonas gingivalis* through regulating the NLRP3 inflammasome,” *Oral Diseases*, vol. 25, no. 8, pp. 2030–2039, 2019.
- [51] X. Wu, Y. Wang, T. Yu et al., “Blocking MIR155HG/miR-155 axis inhibits mesenchymal transition in glioma,” *Neuro-Oncology*, vol. 19, no. 9, pp. 1195–1205, 2017.
- [52] J. Kim, K. S. Lee, J. H. Kim et al., “Aspirin prevents TNF- α -induced endothelial cell dysfunction by regulating the NF- κ B-dependent miR-155/eNOS pathway: role of a miR-155/eNOS axis in preeclampsia,” *Free Radical Biology & Medicine*, vol. 104, pp. 185–198, 2017.
- [53] N. Li, Y. Liu, and J. Cai, “LncRNA MIR155HG regulates M1/M2 macrophage polarization in chronic obstructive pulmonary disease,” *Biomedicine & Pharmacotherapy*, vol. 117, article 109015, 2019.
- [54] X. Wang, J. Liu, Z. Dai, and Y. Sui, “Andrographolide improves PCP-induced schizophrenia-like behaviors through blocking interaction between NRF2 and KEAP1,” *Journal of Pharmacological Sciences*, vol. 147, no. 1, pp. 9–17, 2021.
- [55] J. Y. Seo, E. Pyo, J.-P. An, J. Kim, S. H. Sung, and W. K. Oh, “Andrographolide activates Keap1/Nrf2/ARE/HO-1 pathway in HT22 cells and suppresses microglial activation by Abeta42 through Nrf2-related inflammatory response,” *Mediators of Inflammation*, vol. 2017, Article ID 5906189, 12 pages, 2017.
- [56] E. Yoshihara, S. Masaki, Y. Matsuo, Z. Chen, H. Tian, and J. Yodoi, “Thioredoxin/Txnip: redoxisome, as a redox switch for the pathogenesis of diseases,” *Frontiers in Immunology*, vol. 4, 2014.
- [57] H. Y. Sun, Y. J. Hu, X. Y. Zhao et al., “Age-related changes in mitochondrial antioxidant enzyme Trx2 and TXNIP-Trx2-ASK1 signal pathways in the auditory cortex of a mimetic aging rat model: changes to Trx2 in the auditory cortex,” *The FEBS Journal*, vol. 282, no. 14, pp. 2758–2774, 2015.
- [58] W. Xu, L. Wang, J. Li, Y. Cai, and Y. Xue, “TXNIP mediated the oxidative stress response in glomerular mesangial cells partially through AMPK pathway,” *Biomedicine & Pharmacotherapy*, vol. 107, pp. 785–792, 2018.
- [59] L. Wang, H. Zhao, H. Xu et al., “Targeting the TXNIP-NLRP3 interaction with PSSM1443 to suppress inflammation in sepsis-induced myocardial dysfunction,” *Journal of Cellular Physiology*, vol. 236, no. 6, pp. 4625–4639, 2021.
- [60] S. B. Kovacs and E. A. Miao, “Gasdermins: effectors of pyroptosis,” *Trends in Cell Biology*, vol. 27, no. 9, pp. 673–684, 2017.
- [61] M.-X. Duan, H. Zhou, Q.-Q. Wu et al., “Andrographolide protects against HG-induced inflammation, apoptosis, migration, and impairment of angiogenesis via PI3K/AKT-eNOS signaling in HUVECs,” *Mediators of Inflammation*, vol. 2019, Article ID 6168340, 15 pages, 2019.
- [62] Y. Peng, Y. Wang, N. Tang et al., “Andrographolide inhibits breast cancer through suppressing COX-2 expression and angiogenesis via inactivation of p300 signaling and VEGF pathway,” *Journal of Experimental & Clinical Cancer Research*, vol. 37, no. 1, p. 248, 2018.
- [63] Y. Li, Y. Fu, J. Sun et al., “Tanshinone IIA alleviates NLRP3 inflammasome-mediated pyroptosis in *Mycobacterium tuberculosis*-(H37Ra-) infected macrophages by inhibiting

- endoplasmic reticulum stress,” *Journal of Ethnopharmacology*, vol. 282, article 114595, 2022.
- [64] Y. Li, W. Song, Y. Tong et al., “Isoliquiritin ameliorates depression by suppressing NLRP3-mediated pyroptosis via miRNA-27a/SYK/NF- κ B axis,” *Journal of Neuroinflammation*, vol. 18, no. 1, p. 1, 2021.
- [65] Y. Zhang, X. Liu, X. Bai et al., “Melatonin prevents endothelial cell pyroptosis via regulation of long noncoding RNA MEG3/miR-223/NLRP3 axis,” *Journal of Pineal Research*, vol. 64, no. 2, 2018.
- [66] M. V. Rajaram, B. Ni, J. D. Morris et al., “Mycobacterium tuberculosis lipomannan blocks TNF biosynthesis by regulating macrophage MAPK-activated protein kinase 2 (MK2) and microRNA miR-125b,” *Proceedings of the National Academy of Sciences of the United States of America*, vol. 108, no. 42, pp. 17408–17413, 2011.
- [67] C. Wan, R. Han, L. Liu et al., “Role of miR-155 in fluorooctane sulfonate-induced oxidative hepatic damage via the Nrf2-dependent pathway,” *Toxicology and Applied Pharmacology*, vol. 295, pp. 85–93, 2016.
- [68] N. J. Roos, U. Duthaler, J. Bouitbir, and S. Krähenbühl, “The uricosuric benzbromarone disturbs the mitochondrial redox homeostasis and activates the NRF2 signaling pathway in HepG2 cells,” *Free Radical Biology & Medicine*, vol. 152, pp. 216–226, 2020.
- [69] Y. Lou, Z. Guo, Y. Zhu et al., “Houttuynia cordata Thunb. and its bioactive compound 2-undecanone significantly suppress benzo(a)pyrene-induced lung tumorigenesis by activating the Nrf2-HO-1/NQO-1 signaling pathway,” *Journal of Experimental & Clinical Cancer Research*, vol. 38, no. 1, p. 242, 2019.
- [70] C. Y. Wang, Y. Xu, X. Wang, C. Guo, T. Wang, and Z. Y. Wang, “DI-3-n-Butylphthalide inhibits NLRP3 inflammasome and mitigates Alzheimer’s-like pathology via Nrf2-TXNIP-TrX Axis,” *Antioxidants & Redox Signaling*, vol. 30, no. 11, pp. 1411–1431, 2019.
- [71] X. Chen, G. Liu, Y. Yuan, G. Wu, S. Wang, and L. Yuan, “NEK7 interacts with NLRP3 to modulate the pyroptosis in inflammatory bowel disease via NF- κ B signaling,” *Cell Death & Disease*, vol. 10, no. 12, p. 906, 2019.
- [72] R. Verma, S. M. Pinto, A. H. Patil et al., “Quantitative proteomic and phosphoproteomic analysis of H37Ra and H37Rv strains of Mycobacterium tuberculosis,” *Journal of Proteome Research*, vol. 16, no. 4, pp. 1632–1645, 2017.
- [73] H. Zheng, L. Lu, B. Wang et al., “Genetic basis of virulence attenuation revealed by comparative genomic analysis of Mycobacterium tuberculosis strain H37Ra versus H37Rv,” *PLoS One*, vol. 3, no. 6, article e2375, 2008.